

DEUTERON MAGNETIC RESONANCE

OF TTF(d₀)-TCNQ(d₄)

by

PHILIP ROMAN KUBIK

B.Sc., University of British Columbia, 1974

A THESIS SUBMITTED IN PARTIAL FULFILLMENT
OF THE REQUIREMENTS FOR THE DEGREE OF
MASTER OF SCIENCE

in

THE FACULTY OF GRADUATE STUDIES
DEPARTMENT OF PHYSICS

We accept this thesis as conforming
to the required standard

THE UNIVERSITY OF BRITISH COLUMBIA

April, 1977

© Philip Roman Kubik, 1977

In presenting this thesis in partial fulfilment of the requirements for an advanced degree at the University of British Columbia, I agree that the Library shall make it freely available for reference and study.

I further agree that permission for extensive copying of this thesis for scholarly purposes may be granted by the Head of my Department or by his representatives. It is understood that copying or publication of this thesis for financial gain shall not be allowed without my written permission.

Department of Physics

The University of British Columbia
2075 Wesbrook Place
Vancouver, Canada
V6T 1W5

Date April, 1977

ABSTRACT

The deuteron magnetic resonance of powdered TTF(d₀)-TCNQ(d₄) has been observed at 4.2 K and 1.3 K. The lineshape is characterized by a quadrupole splitting with a coupling constant $e^2qQ/h=180.0\pm.7$ kHz and an asymmetry parameter $\eta=.080\pm.002$. The charge density waves (CDW) that are proposed to exist in TTF-TCNQ below 54 K will modulate e^2qQ/h if they occur on the TCNQ chains. This will be manifested by a characteristic broadening of the spectrum. Although the broadening is a factor of 2.4 greater than the expected dipolar broadening, it does not seem that the extra broadening can be ascribed to the presence of a CDW. We can only estimate an upper limit of $\sim 5\%$ for the CDW amplitude based of the observed broadening and the differences in the quadrupole coupling constants of TTF(d₀)-TCNQ(d₄) and TCNQ(d₄).

TABLE OF CONTENTS

	<u>Page</u>
ABSTRACT	ii
TABLE OF CONTENTS	iii
LIST OF TABLES	iv
LIST OF FIGURES	v
ACKNOWLEDGEMENT	vi
CHAPTER	
I INTRODUCTION	1
II DEUTERON MAGNETIC RESONANCE LINESHAPE	12
III EXPERIMENTAL DESIGN AND PROCEDURE	
1) General Description	19
2) Signal:Noise Optimization	22
3) The Tuned Circuit	25
4) Field Sweep and Modulation	30
5) Homogeneity	36
IV RESULTS	38
V SOURCES OF BROADENING	48
VI CONCLUSIONS	59
BIBLIOGRAPHY	61

LIST OF TABLES

<u>Table</u>		<u>Page</u>
I	Quadrupole Coupling Constants and Asymmetry Parameters	46
II	Gross Atomic Charges	56

LIST OF FIGURES

<u>Figure</u>		<u>Page</u>
1	One dimensional, half-filled energy band	3
2	A CDW in a one dimensional lattice	3
3	TTF and TCNQ molecules	5
4	Unit cell of TTF-TCNQ	6
5	Elastic neutron scattering	8
6	a) Laboratory and principal axis coordinate systems	14
	b) Single crystal DMR lineshape	
	c) Effect of averaging over all crystal orientations on the DMR lineshape	
7	Gaussian broadened DMR lineshape	16
8	Effect of a CDW on the DMR spectrum	18
9	Block diagram of the apparatus	21
10	Schematic cut-away diagram of the bottom end of the cryostat	26
11	Tuned circuit and matching network	28
12	Position of the rotating coil probe	35
13	Main peak of TTF(d_0)-TCNQ(d_4) derivative signal	39
14	Outer peak of TTF(d_0)-TCNQ(d_4) derivative signal	40
15	Integral of Fig. 13	41
16	Main peak of TCNQ(d_4) derivative signal	44
17	Proton absorption signal of TTF(d_4)TCNQ(d_0)	50

ACKNOWLEDGEMENT

I gratefully acknowledge the support and encouragement of Dr. W. N. Hardy. All of the samples used in this project were cheerfully provided by Dr. L. Weiler and his co-workers. Finally I wish to thank the National Research Council of Canada for a Postgraduate Scholarship.

Chapter I

INTRODUCTION

Tetrathiofulvalene-tetracyanoquinodimethane (TTF-TCNQ) is a charge transfer complex that exhibits many of the properties of a quasi one dimensional (1D) system. Thus TTF-TCNQ appears to offer the opportunity for experimental verification of 1D theories. A very extensive review of TTF-TCNQ and other highly anisotropic systems is given by André, Bieber, and Gautier (1976).

Strictly 1D systems have some unique properties. Peierls (1955) pointed out that a partially filled 1D electron band is unstable with respect to a static lattice distortion known as the Peierls instability. Consider an electronic band for a 1D lattice with lattice constant b , which is filled up to the Fermi momentum k_F as shown in Fig. 1a. If there are ρ electrons per lattice site then k_F is given by:

$$2k_F = \frac{\rho}{b} \quad \text{I-1}$$

The electronic density of states $N(E)$ for the band is shown in Fig. 1b. For such a band the electronic energy can always be lowered by a periodic lattice distortion. Maximum energy reduction occurs if the wave vector of the distortion is $2k_F$, resulting in a superlattice with a lattice constant $\frac{2b}{\rho}$. This opens a gap of width Δ in the band structure at $\pm k_F$. The lattice distortion produces a potential with the superlattice period. The electronic density is modulated by the potential causing a charge density wave (CDW).

The lowering of the electronic energy must compete with the increase in elastic energy caused by the distortion. For a simple tight binding model, which is suitable for a narrow band system such as TTF-TCNQ, the former always outweighs the latter at low temperatures (Berlinsky, 1976) so that one expects a periodic lattice distortion to occur.

Two cases can be distinguished which depend upon whether or not ρ is a rational number. If it is, the superlattice contains a rational number of lattice sites: the CDW is commensurate with the lattice. Two equivalent configurations for the case $\rho = \frac{1}{2}$ are depicted in Figs. 2a and c. In Fig. 2c the CDW is shifted by b with respect to the configuration in Fig. 2a but the energy is the same. However, the intermediate configuration in which the CDW is translated by $b/2$ has higher energy because the ion cores don't know which way to distort. Therefore the CDW is pinned to the lattice.

Fig. 2b corresponds to the case in which ρ is irrational so the CDW is incommensurate with the lattice. No matter how the CDW is translated, the ion cores can distort slightly to produce a configuration of the same energy. If there were no defects or impurities to pin the CDW, a superconducting state would result because the CDW is too massive to be scattered by phonons. However, a CDW in a 1D system would be particularly susceptible to such pinning.

The foregoing discussion neglects any mention of fluctuation effects which are very important for 1D systems. In fact there is a theorem (Landau and Lifshitz, 1969) which states that 1D systems with forces of finite range, as in the tight

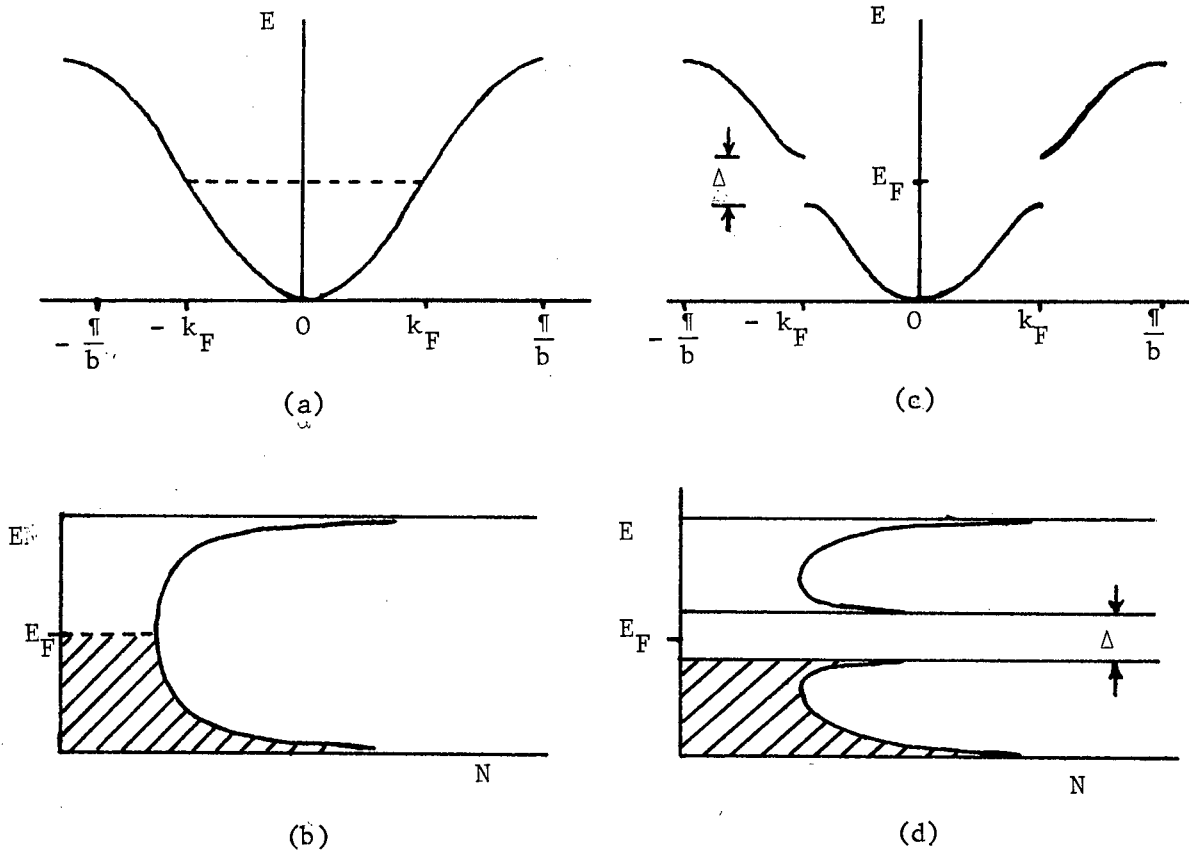


Figure 1) One dimensional, half-filled energy band with a) lattice constant b and b) with a Peierls distortion with wave vector $2k_F$. The respective densities of states are shown in c) and d).

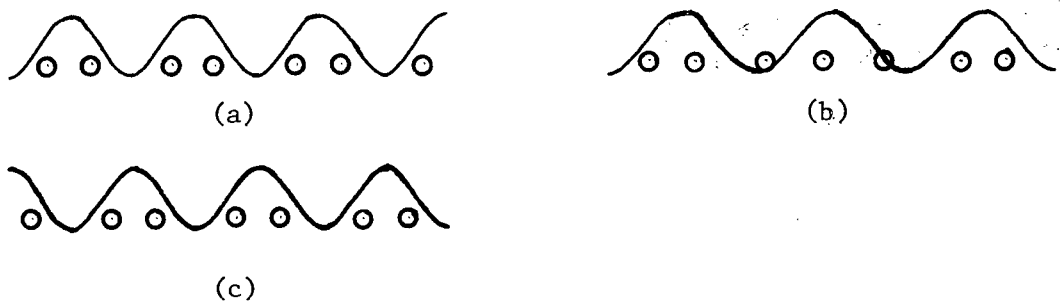


Figure 2) A CDW in a 1D lattice. a) Commensurate CDW with $\rho = \frac{1}{2}$. b) Incommensurate CDW c) A configuration energetically equivalent to a) in which the CDW is displaced by b .

binding model, cannot undergo a phase transition at a finite temperature because of fluctuations.

No real system can be truly 1D. The closest that one can come is a system of weakly coupled chains. Such a system can undergo a 3D phase transition at a finite temperature (Pincus, 1975).

TTF and TCNQ are both planar organic molecules; they are shown in Fig. 3. In the TTF-TCNQ crystal, they stack to form separate TTF and TCNQ chains parallel to the crystal b axis (see Fig. 4b). The unit cell of TTF-TCNQ, containing 4 molecules, is shown in Fig. 4. The crystal structure is monoclinic with space group $P2_1/c$ (Kistenmacher, Phillips, and Cowan, 1973).

Molecular orbital calculations (Berlinsky, Carolan and Weiler, 1974, and references given there) show that the highest occupied molecular orbitals, the ones that form the conduction band, are π orbitals. These are odd under reflection through the plane of the molecule and overlap strongly. This leads to a strong interaction down each chain but the interchain coupling is weak resulting in a quasi 1D system.

The quasi 1D nature of TTF-TCNQ is evinced most notably in the DC conductivity. At room temperature TTF-TCNQ is one of a small group of highly anisotropic organic conductors. The b axis conductivity at room temperature is $\sim 500 (\Omega \text{ cm})^{-1}$. Typical organic insulators have conductivities $\sim 10^{-10}$ to $10^{-14} (\Omega \text{ cm})^{-1}$ whereas copper has $1.7 \times 10^6 (\Omega \text{ cm})^{-1}$. The transverse conductivities of TTF-TCNQ are two orders of magnitude lower.

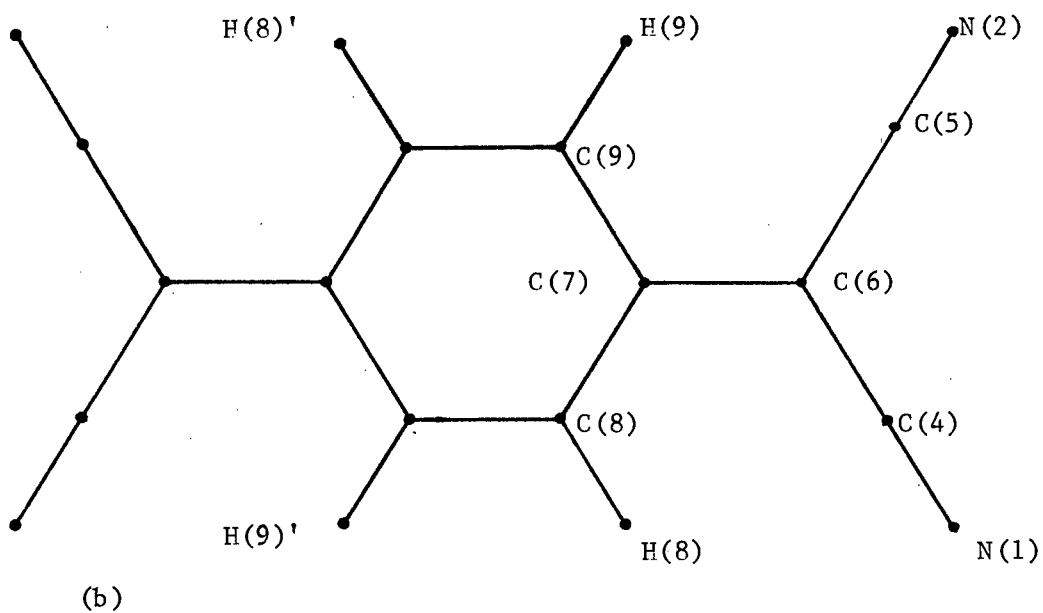
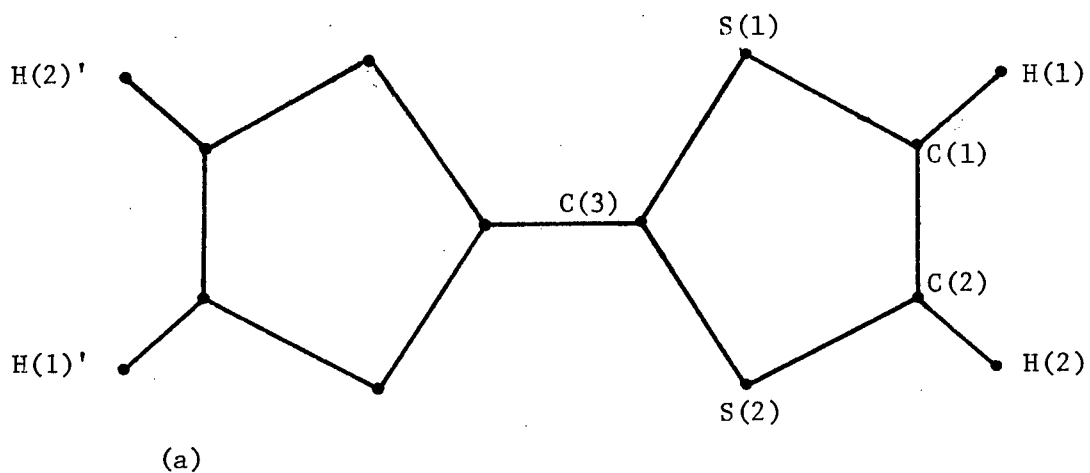
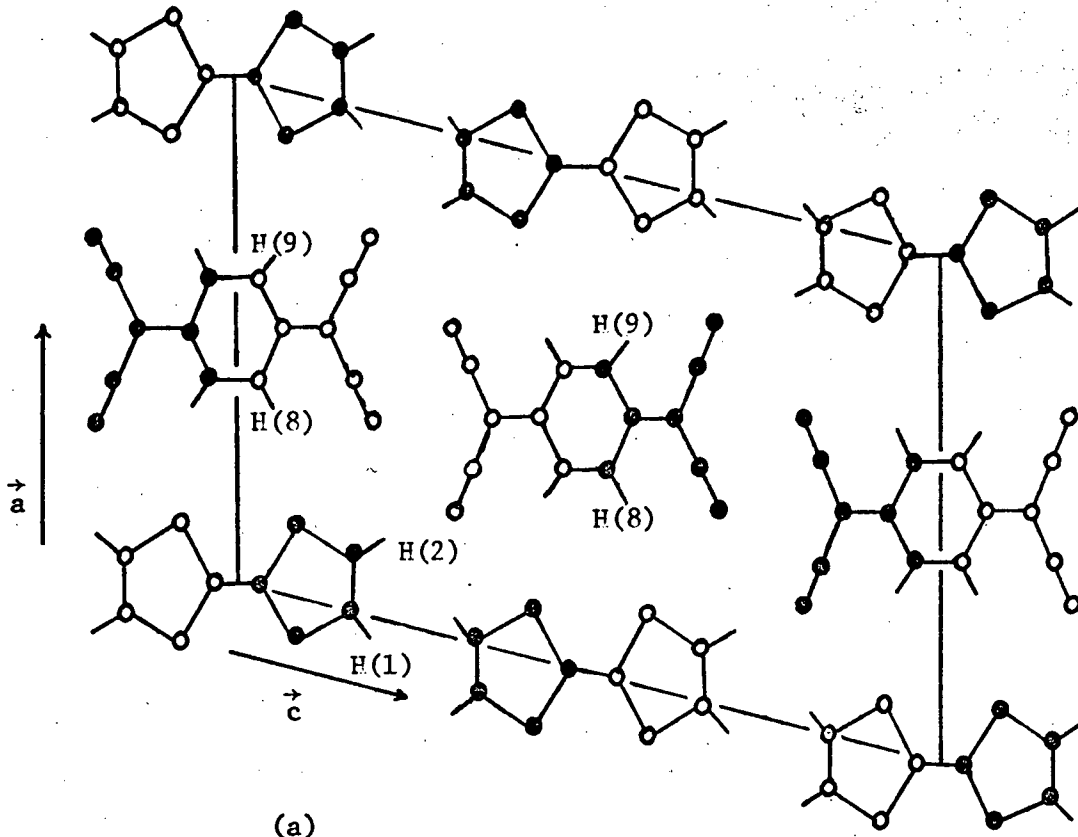
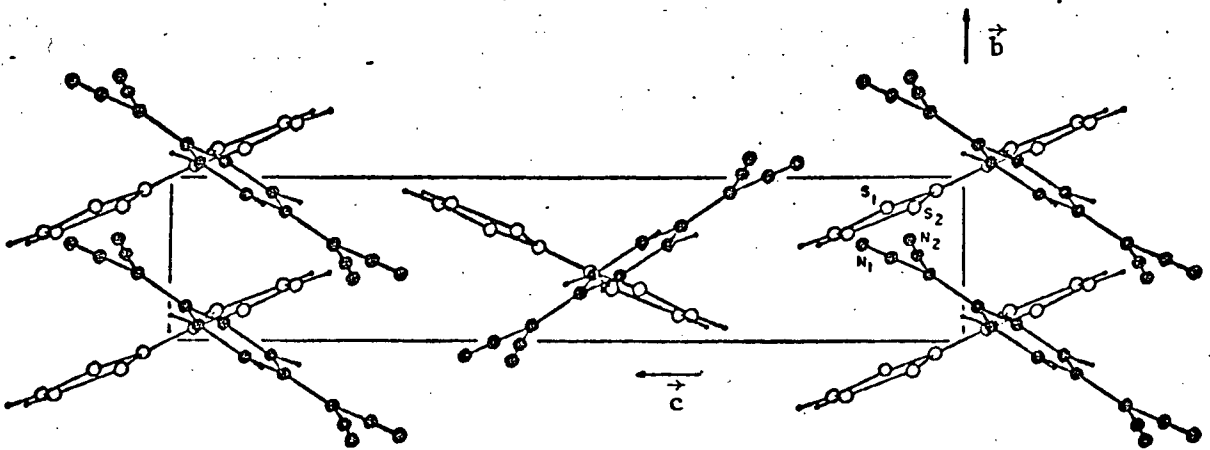


Figure 3) a) TTF molecule. b) TCNQ molecule. The scale is $1.5 \times 10^8 : 1$.



(a)



(b)

Figure 4) Unit cell of TTF-TCNQ. a) View down the b axis. The molecules at $z=c/2$ have their centroids at $y=b/2$. b) View down the c^* axis. The dimensions of the unit cell are (12.3, 17.9, 3.8) Å.

The DC conductivity (Tiedje, 1975) has an approximately T^{-2} dependence (as opposed to T^{-1} for normal pure metals) from 300 K down to about 80 K. A metal-insulator transition occurs at about 54 K and the conductivity plummets. At low temperatures TTF-TCNQ behaves like a small gap semiconductor.

Evidence of a phase transition is also given by susceptibility (Scott et al, 1974), thermopower (Chaikin et al, 1973) and specific heat (Craven et al, 1974) measurements. The DC conductivity, thermopower and more recent specific heat measurements (Djurek et al, 1977) also show the existence of another phase transition at 38 K. The specific data show in addition transitions at 46 K and \sim 48-49 K.

Considerable light was thrown on the nature of the transitions by diffraction studies using diffuse X-ray scattering at $2k_F$ (Denoyer et al, 1975 and Kagoshima et al, 1975) and elastic neutron scattering at $2k_F$ (Comès et al, 1976). Below 38 K there is a 3D superlattice with long range order and a modulation period of $(4\vec{a} \times 3.4\vec{b} \times \vec{c})$. It appears to be incommensurate along the chains. Diffuse X-ray scattering indicates that the distortion is sinusoidal and that the polarization of the distortion is in the \vec{b} direction. The neutron results appear to indicate a small \vec{c} component though this is rather inconclusive. The modulation in the \vec{b} direction is unchanged up to 54 K. The modulation period in the \vec{a} direction drops sharply at 38 K and then more gradually to $2a$ at 54 K as shown in Fig. 5b. The peak intensity, which is proportional to the square of the amplitude of the distortion, drops to the background level at about 54 K as shown in Fig. 5a. In addition, between 38 K and 54 K the peak broadens somewhat in the \vec{a}^* direction indicating some loss of long range order. Its width

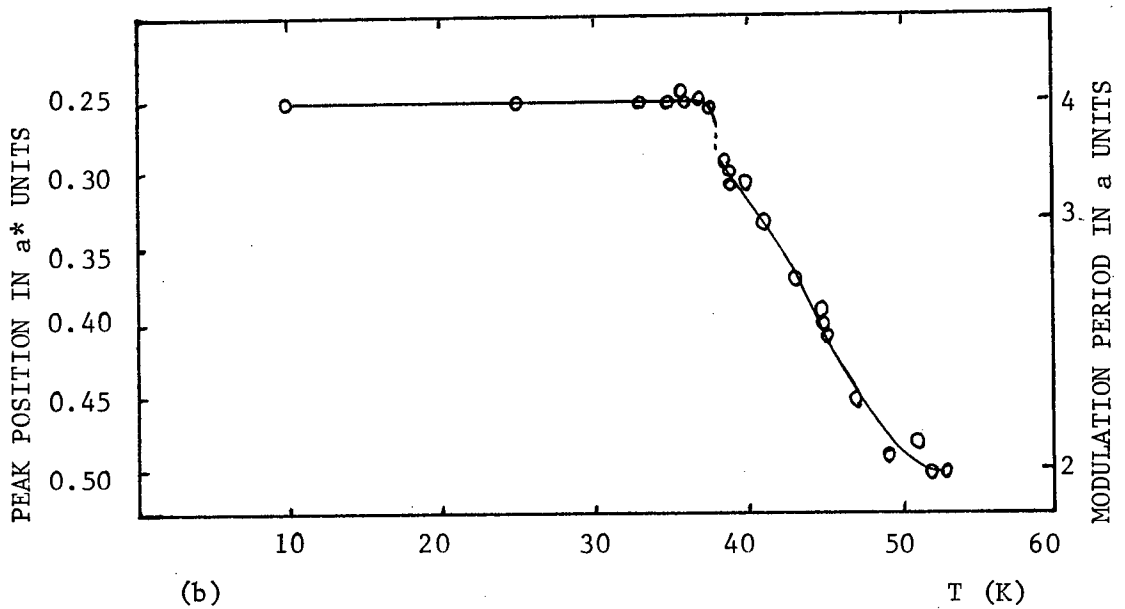
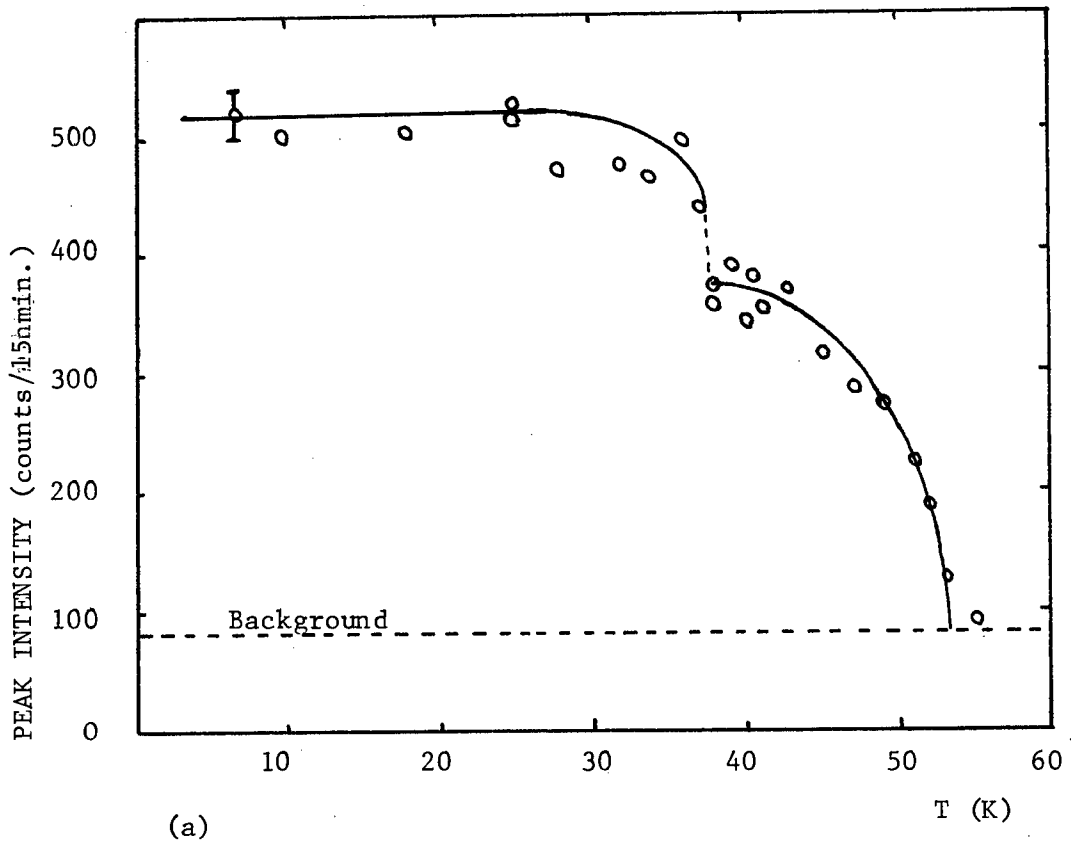


Figure 5) Elastic neutron scattering. a) Peak intensity. b) Modulation period.

is resolution limited in the \vec{b}^* and \vec{c}^* directions throughout the range implying correlation lengths $> 100 \text{ \AA}^0$.

Elastic neutron scattering in particular is in principle capable of giving much more information on the nature of structure changes between the transitions. However, because the satellite peaks are very much weaker than the Bragg peaks very little information has been obtained from the intensities. Apart from the rather inconclusive information about the polarization of the distortion mentioned above, there are only two results of note. First, the TTF and TCNQ molecules appear to be modulated as units: the distortion is intermolecular rather than intramolecular. Secondly, the amplitude of the distortion has been roughly estimated to be 1%.

The occurrence of a Peierls distortion at 54 K is well established. It isn't clear though whether the distortion occurs on the TTF chains, the TCNQ chains, or both. Neither is it clear why the modulation in the a direction and the peak intensity have the temperature dependences shown in Fig. 5. Of particular interest is the nature of the first order phase transition at 38 K.

Since not much more structural information can be expected from diffraction studies until larger crystals are available, one must look to other techniques. It was mentioned above that the lattice distortion is accompanied by a CDW with the same modulation period. This opens up a new avenue by allowing one to study the transitions by probing the electric field. One means of doing this is by examining the nuclear magnetic resonance (NMR) spectra of any nuclei in TTF-TCNQ with

a quadrupole moment. The hamiltonian for the interaction of such a nucleus with an electrostatic potential can be written as a multipole expansion. The expansion will contain a term involving the product of the electric field gradient (EFG) and the nuclear quadrupole moment. This term causes a splitting of the NMR lineshape which is proportional to the EFG at the nucleus being probed.

The only nucleus in TTF-TCNQ with a non-zero quadrupole moment Q and a natural abundance greater than 1% is N^{14} . Since it occurs only in TCNQ, only those chains can be probed. No N^{14} quadrupole resonance studies have been made for TTF-TCNQ though some have been done on K-TCNQ (Murgich and Pissanetzky, 1973).

One can evade the problem of the paucity of quadrupolar nuclei by replacing some of the nuclei that have $Q = 0$ with isotopes that have $Q \neq 0$. The electronic states would be affected negligibly by such a change. For most nuclei this would be very difficult and expensive but the H atoms can be replaced by deuterons relatively easily. One can go so far as to selectively deuterate either the TTF or the TCNQ molecules. Each of them contains 4 protons in positions that are equivalent in the molecule (Fig. 3). Since the deuteron magnetic resonance (DMR) of selectively deuterated samples of TTF-TCNQ can potentially give more information than N^{14} quadrupole resonance, the former approach was taken in this study.

The quadrupole moment of the deuteron is too small to allow the use of nuclear quadrupole resonance in zero magnetic field as could be done for N^{14} . However, one can observe the quadrupole splitting of the high field NMR lineshape.

Ideally one would like to observe the DMR spectrum of a single crystal of deuterated TTF-TCNQ as the temperature was varied in the region of the transitions. Given the small size of single crystals of TTF-TCNQ available when this project was begun, single crystal DMR did not seem feasible. All of the work described here employed powder samples which have a much more complicated spectrum than single crystals because the absorption frequencies depend on the crystal orientation.

The DMR spectrum of TTF(d_0)-TCNQ(d_4) has been observed at 1.3 K and 4.2 K. An unsuccessful attempt was also made at 77 K. Even at liquid helium temperatures long signal averaging was required. Therefore it seems unlikely that the experiment in its present form can be adapted to study the temperature region of the phase transitions.

The X-ray and neutron diffraction studies show that below 38 K an incommensurate CDW should be established along the chains. The DMR lineshape shows no obvious manifestation of a CDW on the TCNQ chains; we can at best place an upper limit of 5% on the CDW amplitude.

Further work on TTF(d_4)-TCNQ(d_0) is in progress.

Chapter II

THE DEUTERON MAGNETIC RESONANCE LINESHAPE

Good discussions of the effects of electric quadrupole interactions on NMR lineshapes are given by Abragam (1961) and Slichter (1963). A brief recapitulation will be given here.

In a magnetic field H, the hamiltonian for a nucleus with spin I and quadrupole moment Q is:

$$\mathcal{H} = \gamma \hbar \vec{H} \cdot \vec{I} + \frac{e^2 q Q}{4I(2I-1)} [3I_z^2 - I(I+1) + \frac{1}{2}\eta(I_+^2 + I_-^2)] \quad \text{II-1}$$

where the coordinate system is chosen so that if V is the electrostatic potential, the x, y, z axes are the principal axes of the EFG tensor such that $|V_{zz}| \geq |V_{yy}| \geq |V_{xx}|$.

$$eq = V_{zz}$$

$$\eta = \frac{V_{xx} - V_{yy}}{V_{zz}}$$

γ = nuclear gyromagnetic ratio

$$I_+ = I_x + iI_y$$

$$I_- = I_x - iI_y$$

The first term is the Zeeman interaction and the second is the quadrupole interaction. eq is the maximum component of the EFG tensor in the principal axis system. η , the asymmetry parameter, measures the asymmetry of the EFG about the z axis. eq and η completely specify the EFG tensor in the principal axis system because V must satisfy Poisson's equation.

We now define another coordinate system X,Y,Z such that \vec{H} lies along the Z axis as shown in Fig. 6a. θ is the angle between the z and Z axes while ψ is the angle between the x and X axes.

In a strong magnetic field, the quadrupole interaction can be treated by first order perturbation theory. For a deuteron, the quadrupole moment is quite small so fields of a few kilogauss are sufficiently strong. The transition frequencies for a spin 1 nucleus such as the deuteron are:

$$f = f_0 \pm \alpha(\eta, \theta, \psi) f_Q \quad \text{II-2}$$

$$\text{where } f_0 = \gamma H_Z$$

$$f_Q = 3/2 e^2 q Q / h$$

$$= 3 \cos^2 \theta - 1 + \eta \cos(2\psi) (\cos^2 \theta - 1)$$

f_0 is the Larmor frequency and f_Q is 3/2 times the quadrupole coupling constant (QCC).

For a single crystal in which all deuteron sites are equivalent, the NMR absorption spectrum consists of two peaks as shown in Fig. 6b. The broadening of each peak will normally be determined by the dipole-dipole interactions between the spins.

If one has a powder sample, one must average over all orientations of the crystal axes with respect to the magnetic field. The resulting lineshapes are given by elliptic integrals (Cohen and Reif, 1957). The effect of averaging on the unbroadened lower peak is shown in Fig. 6c for several values of η (Barnes and Bloom, 1972). The upper peak gives a lineshape that is identical except that it is reflected through f_0 . If

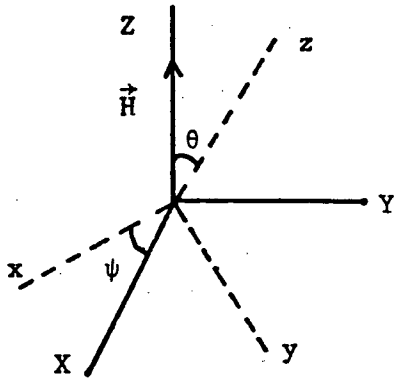
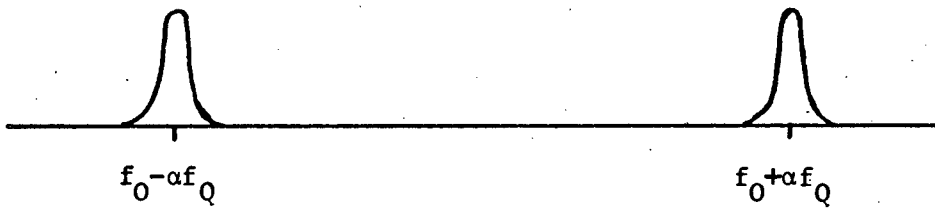


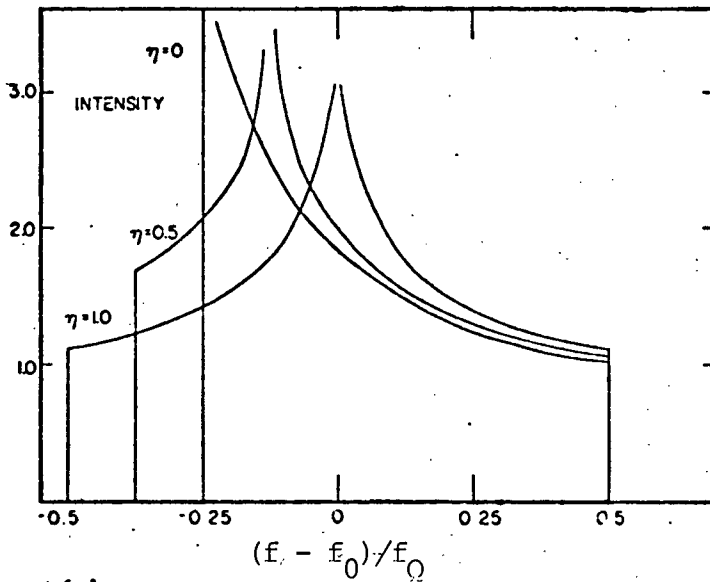
Figure 6) a) Laboratory coordinate system (solid) and EFG tensor principal axes (dashed).

(a)



(b)

Single crystal DMR lineshape with all spins equivalent.



(c)

Effect of averaging over all crystal orientations for the lower peak of b) (Barnes and Bloom, 1972).

$\eta \neq 0$, there are three main features: a singularity at $f_0 - \frac{1}{4}f_Q (1 - \eta)$, a shoulder at $f_0 - \frac{1}{4}f_Q (1 + \eta)$ and a step at $f_0 + \frac{1}{2}f_Q$. If $\eta = 0$, the singularity and shoulder merge.

In order to see the effect of gaussian broadening, Barnes and Bloom (1972) have generated the lineshapes synthetically using a computer. The complete unbroadened spectrum is shown by the circles in Fig. 7a for $\eta = .18$. The effect of gaussian broadening is shown by the solid line. In this experiment the derivative of the absorption was detected: this is shown in Fig. 7b. To a very good approximation, the small outer peaks occur at $f_0 \pm \frac{1}{2}f_Q$, the main peaks at $f_0 \mp \frac{1}{4}f_Q (1 - \eta)$, and the baseline crossings at $f_0 \mp \frac{1}{4}f_Q (1 + \eta)$. η and the QCC can be found after identification of any two of these features.

Now consider the effect of a CDW on the single crystal lineshape shown in Fig. 6b. The simplest case is that of a 1D sinusoidal, commensurate CDW with a superlattice period nb where n is an integer. In general the EFG will have n different values at the nuclei so each of the two lines of Fig. 6b will be split into a group of n satellite lines. The splitting between the new satellites in each group will not be constant and some lines may coincide resulting in a single peak with increased intensity.

Clearly if n is made large, the separation of the satellites in each group will be correspondingly reduced. Eventually that separation will become less than the gaussian broadening and each group of satellites will form a single broadened line.

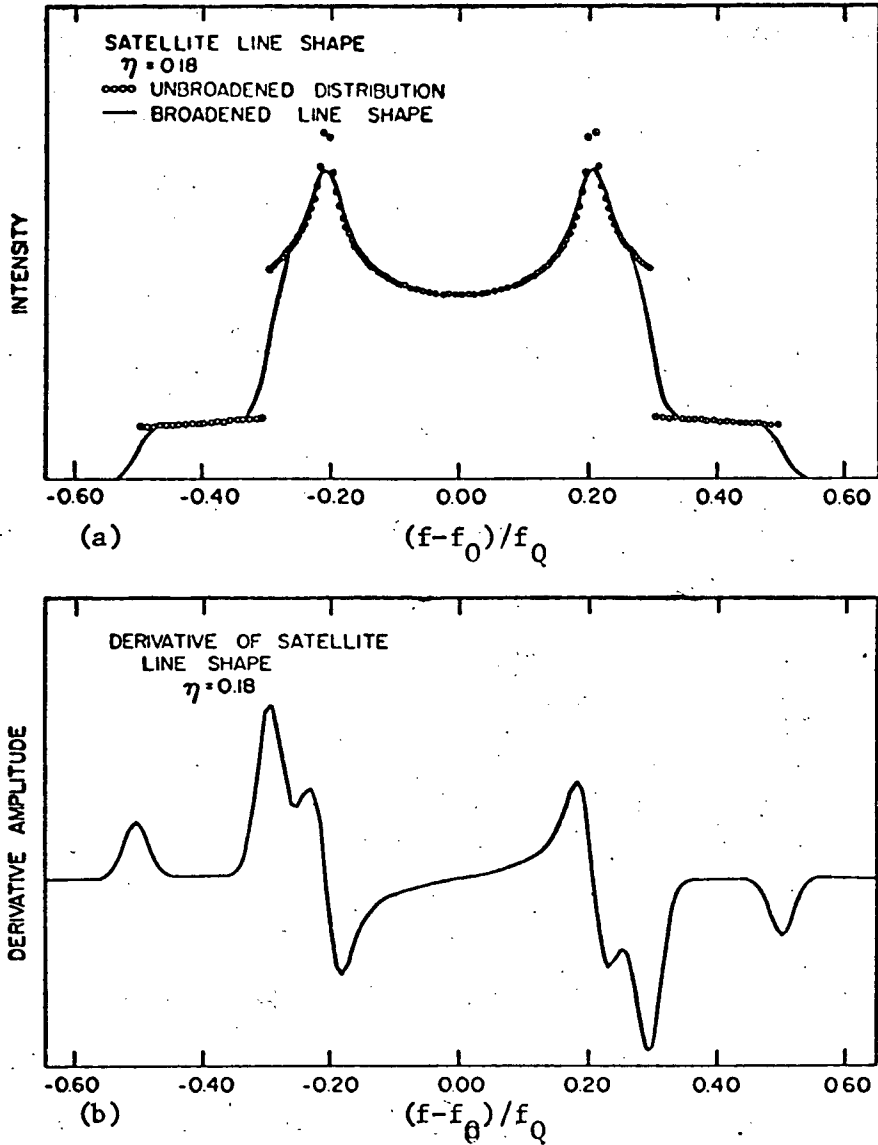


Figure 7) a) Complete DMR absorption lineshape for a powder generated by computer. b) Derivative of a) (Barnes and Bloom, 1972).

A pinned, incommensurate CDW is obtained in the limit as n approaches infinity. Follstaedt and Slichter (1975) have calculated the NMR spectrum for this case. Consider a cubic crystal lattice with a plane sinusoidal CDW of amplitude p and wave vector \vec{Q} . The electron density $n(\vec{r})$ at the point \vec{r} is:

$$n(\vec{r}) = n_0 \{1 + p \cos(\vec{Q} \cdot \vec{r})\} \quad \text{II-3}$$

Poisson's equation gives the EFG to be:

$$eq = -4 \pi p n_0 \cos(\vec{Q} \cdot \vec{r}) \quad \text{II-4}$$

The NMR lineshape $S(f-f_0)$ resulting from the CDW will be:

$$S(f-f_0) = \pi^{-1} \left\{1 - \left(\frac{f-f_0}{\alpha f_M}\right)^2\right\}^{-\frac{1}{2}} \quad \text{II-5}$$

$$\text{where } f_M = 3/2 e^2 q_M Q/h$$

$$\text{and } eq_M = \text{maximum value of } eq$$

$$= 4 \pi p n_0$$

This lineshape is shown in Fig. 8. Qualitatively one would expect a similar shape since more nuclei will experience EFG's in the neighbourhoods of the maxima and minima than near zero. For a powder sample with gaussian broadening, it would be necessary to convolute Fig. 8 with Fig. 7a.

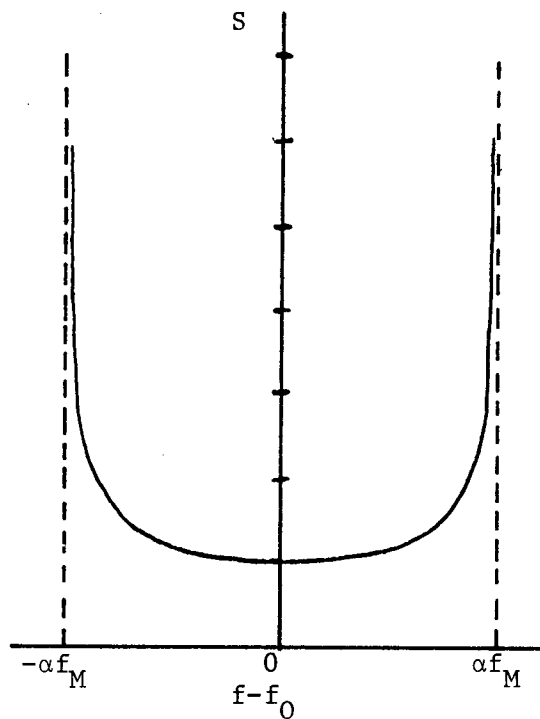


Figure 8) Distribution function $S(f-f_0)$ for a plane, sinusoidal CDW in an isotropic lattice.

Chapter III

EXPERIMENTAL DESIGN AND PROCEDURE

1) General Description

A continuous wave, fixed frequency (8.5 MHz) NMR absorption spectrometer with Q-meter detection was employed for these experiments. RF power was supplied to a high Q parallel resonant circuit by a high output impedance current generator. At the tuned circuit resonance and with no sample, the impedance across the coil is:

$$R = Q \omega L \quad \text{III-1}$$

where $\omega = 2 \pi f$ (resonance frequency)

L = coil inductance

If the NMR sample is placed in the coil and if $Q \gg 1$, the impedance Z becomes (Abragam, 1961):

$$Z = R \{ 1 - i 4 \pi \eta Q \chi (\omega) \} \quad \text{III-2}$$

where η = ratio of the sample volume to the coil volume

= filling factor

$\chi (\omega)$ = complex susceptibility of the sample

$$= \chi'(\omega) - i \chi''(\omega)$$

If the impedance of the current generator is much greater than the tuned circuit impedance, then the relative change in the voltage across the coil is:

$$\Delta V/V = |\Delta Z / Z|$$
$$\approx -4\pi Q \eta \chi''(\omega)$$

III-3

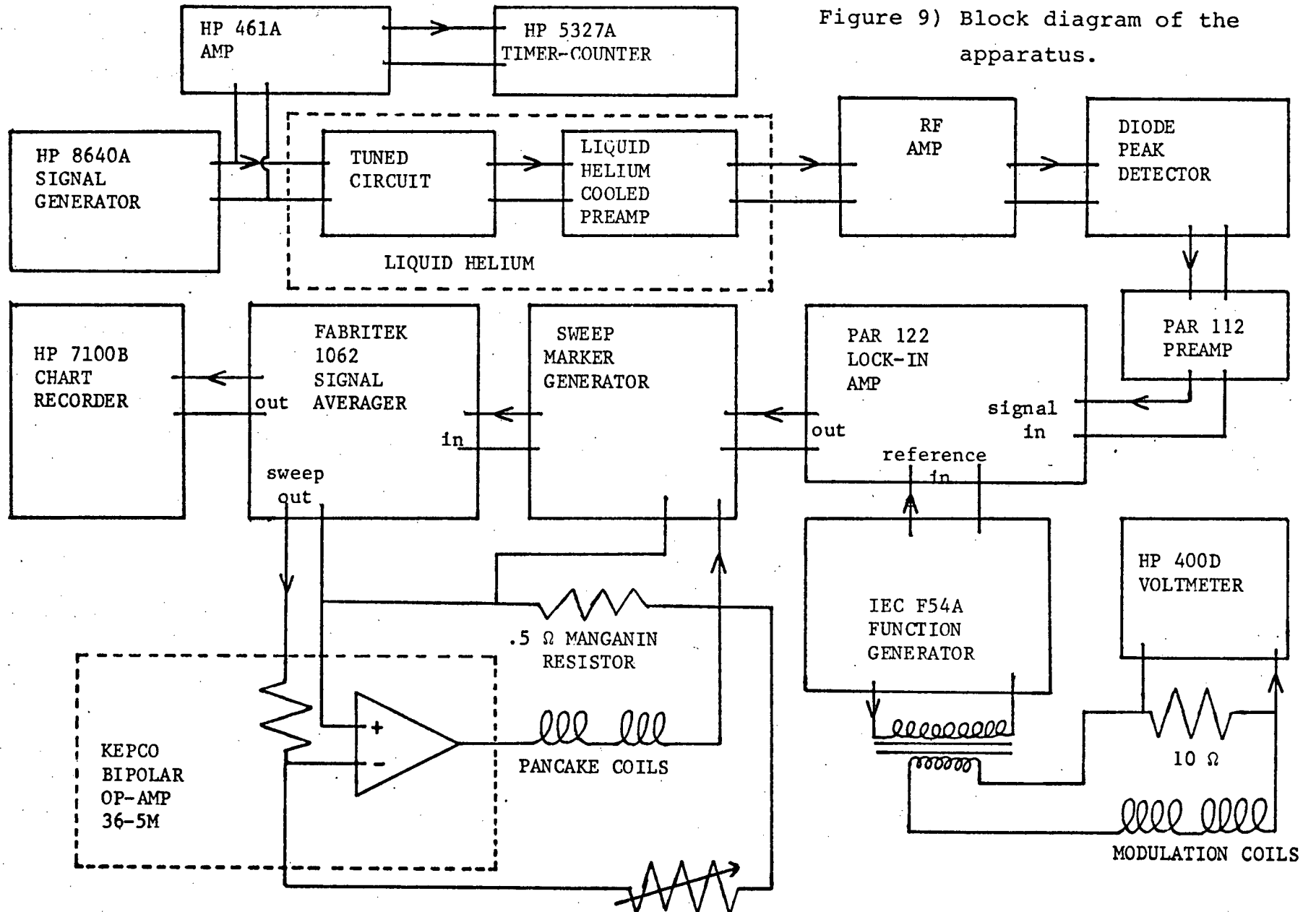
$\Delta V/V$ is proportional to the NMR absorption signal $\chi''(\omega)$.

The tuned circuit voltage V was amplified directly. A bridge was not required to prevent saturation of the preamplifier because of the low RF levels needed to avoid saturation of the resonance.

A block diagram of the apparatus is shown in Fig. 9. A static magnetic field H was applied using a Magnion 9 inch pole piece electromagnet controlled by an FFC-4 Field Regulator with a rotating coil probe. The field was swept slowly, typically through 100 G over 50 s, using disc-shaped "pancake" coils mounted on the pole faces. Small sinusoidal modulation of about 1 G at an audio frequency f_m was applied parallel to H using small coils mounted inside the liquid helium cryostat. The fundamental component of the modulated signal was detected by a PAR 122 lock-in detector so as to obtain the derivative of χ'' .

In order to maximize the signal to noise (S:N) ratio all experiments on TTF-TCNQ were performed in the range 1.3 K to 4.2 K. This made it possible to use a liquid helium cooled preamplifier which had a noise temperature of 8 K when operated at 4.2 K. After the RF signal was amplified by the preamp, it was amplified again at room temperature before going into a diode detector. The signal at the frequency f_m was then detected by the lock-in detector. The output of the lock-in detector was added to two sweep calibration markers in the Sweep Marker Generator and then went into a Fabritek 1062 Signal Averager.

Figure 9) Block diagram of the apparatus.



2) Signal: Noise Optimization

The DMR signal of deuterated TTF-TCNQ is very weak so it is essential to make every effort to maximize the S:N ratio. The weak signal is the result of a number of unfavourable conditions: the density of spins is low (14% of that in H₂O), the packing fraction of the powdered sample is low ($\approx 10\%$), the gyromagnetic ratio of deuterons is small and, finally, one is working with a very broad powder spectrum. Abragam (1961) has given an approximate equation for the S:N ratio of an NMR spectrometer under the following conditions:

- 1) no quadrupole splitting;
- 2) the spin lattice relaxation time T_1 and transverse relaxation time T_2 are equal;
- 3) negligible inhomogeneous broadening by the magnet;
- 4) the RF field is chosen to give the maximum signal. This means that if $2H_1$ is the amplitude of the RF magnetic field, it must satisfy $\gamma^2 H_1^2 T_1 T_2 = 1$.

If Abragam's equation is modified to allow $T_1 \neq T_2$, which is the case for TTF-TCNQ, one gets:

$$S:N \approx \frac{\gamma^2 I(I+1)}{12 F} N \eta \left(\frac{\mu_0 V_C \omega^3 T_2}{2 (kT)^3 \Delta f T_1} \right)^{\frac{1}{2}} \quad \text{III-4}$$

- where
- I = nuclear spin
 - F = noise figure of the detection system
 - N = number of spins/unit volume of the sample
 - V_C = volume of the RF coil
 - Δf = bandwidth of the detection system
 - T = temperature
 - k = Boltzmann's constant

Equation III-1 includes a reduction by $\sqrt{8}$ because the derivative of the absorption is observed (Andrew, 1955).

The parameters which are under the experimenter's control are Q , F , n , V_C , ω , T and Δf . The maximum value of ω that one can use is limited by the available magnetic field (13 kG in these experiments) since $\omega = \gamma H$ at resonance. The equation suggests that it is desirable to make T as low as possible. There are two reasons for this. The static susceptibility $\chi_0 \propto T^{-1}$ and the Johnson noise from the tuned circuit is proportional to $T^{1/2}$. However, the situation is more complicated because both Q and T_1 are temperature dependent.

If the Q were limited only by losses in the coil, it would increase as T decreased because in the normal skin depth region $Q \propto \rho^{-1/2}$ where ρ is the resistivity of the coil material. In practice there will be other losses as well such as dissipation in the capacitor, coil holder, and the outer shield which may or may not decrease as quickly. The Q of the sample resonant circuit described here increased from 95 at room temperature to about 850 at 4.2 K. Since the resistivity of commercial copper decreases by about a factor of 100 over the same temperature range, the losses must be primarily in the copper.

T_1 normally increases as T decreases. For some substances T_1 may increase sufficiently that one is better off working at higher temperatures. However, this is not the case for the DMR signal of TTF-TCNQ. Between 4.2 K and 1.3 K the deuteron relaxation time changed by only a factor of 3/2. This gives an expected improvement in S:N between 4.2 K and 1.3 K of about 5 which was realized in practice. An attempt was made to observe the signal at 77 K to no avail.

Equation III-4 implies that one should make the bandwidth of the detection system as narrow as possible. This can be done either by making the lock-in detector time constant long, which requires a slow sweep rate, or by keeping the time constant short and averaging many fast sweeps in a signal averager. The relative merits of the two techniques are discussed in section III-4.

It has already been mentioned that for TTF-TCNQ the S:N can be improved by cooling the apparatus to liquid helium temperatures because of the factor $Q^{1/2} T^{-3/2}$ in equation III-4. A factor of T^{-1} improvement results from simply cooling the sample. The additional $Q^{1/2} T^{-1/2}$ improvement only arises if the entire tuned circuit is cooled. Consider the case of a parallel resonant circuit where the sample coil is cooled but the tuning capacitor and the preamplifier are not. The preamplifier is assumed to have infinite input resistance but finite input capacitance. It would be necessary to have a coaxial cable between the coil and tuning capacitor. Since the cable goes from 4.2 K to 295 K it would require low thermal conductivity which generally implies a relatively high electrical resistance. This would lower the Q and it would increase the effective noise temperature of the tuned circuit because much of the circuit would be above 4.2 K.

The circuit can be improved by cooling the capacitor but the full benefit is still not achieved because the distributed capacitance of the coaxial cable and the input capacitance of the preamp form part of the tuned circuit. The full effect of the factor $Q^{1/2} T^{-1/2}$ can only be attained by cooling the preamplifier since it forms part of the tuned circuit. In the present system we have used a Ge JFET preamplifier which can be cooled to 4.2 K (Hardy and Gray, 1969). Using an NMR signal, the noise figure of the preamp was measured to be ~ 2 for a matched source resistance

at 4.2 K. This agrees quite well with the results of Hardy and Gray (1969). The cooled preamp does have the disadvantage of increasing the liquid helium boil-off rate. At 4.2 K, about half of the boil-off was due to power dissipation in the preamp.

3) The Tuned Circuit

A diagram of the bottom end of the cryostat is shown in Fig. 10. Its design was governed by three guiding principles: to maximize the Q, to keep H atoms away from the coil so that the proton resonance of TTF-TCNQ could be studied, and to minimize microphonics. The first two objectives were quite successful but, except at the lowest RF and modulation levels used, there remained some microphonic pickup caused by the modulation field.

The coaxial cables at the bottom end of the cryostat were copper and the solder joints in the tuned circuit were made with pure indium solder. Although indium doesn't become superconducting because of the 13 kG magnetic field, it has a very low normal state resistivity at 4.2 K because of its high purity. The inner surfaces of the outer brass shield were electroplated with copper to reduce eddy current losses.

The coil holder was constructed from Teflon because it is a very low loss dielectric and it contains no protons. The modulation coils were constructed from Formvar coated copper wire and cemented in place using a low loss coil coating of dissolved polystyrene. Finally, they were wrapped in Teflon tape. The small residual proton signal that was observed with the sample removed came from the modulation coils and the Bakelite rods screwed into the coil holder.

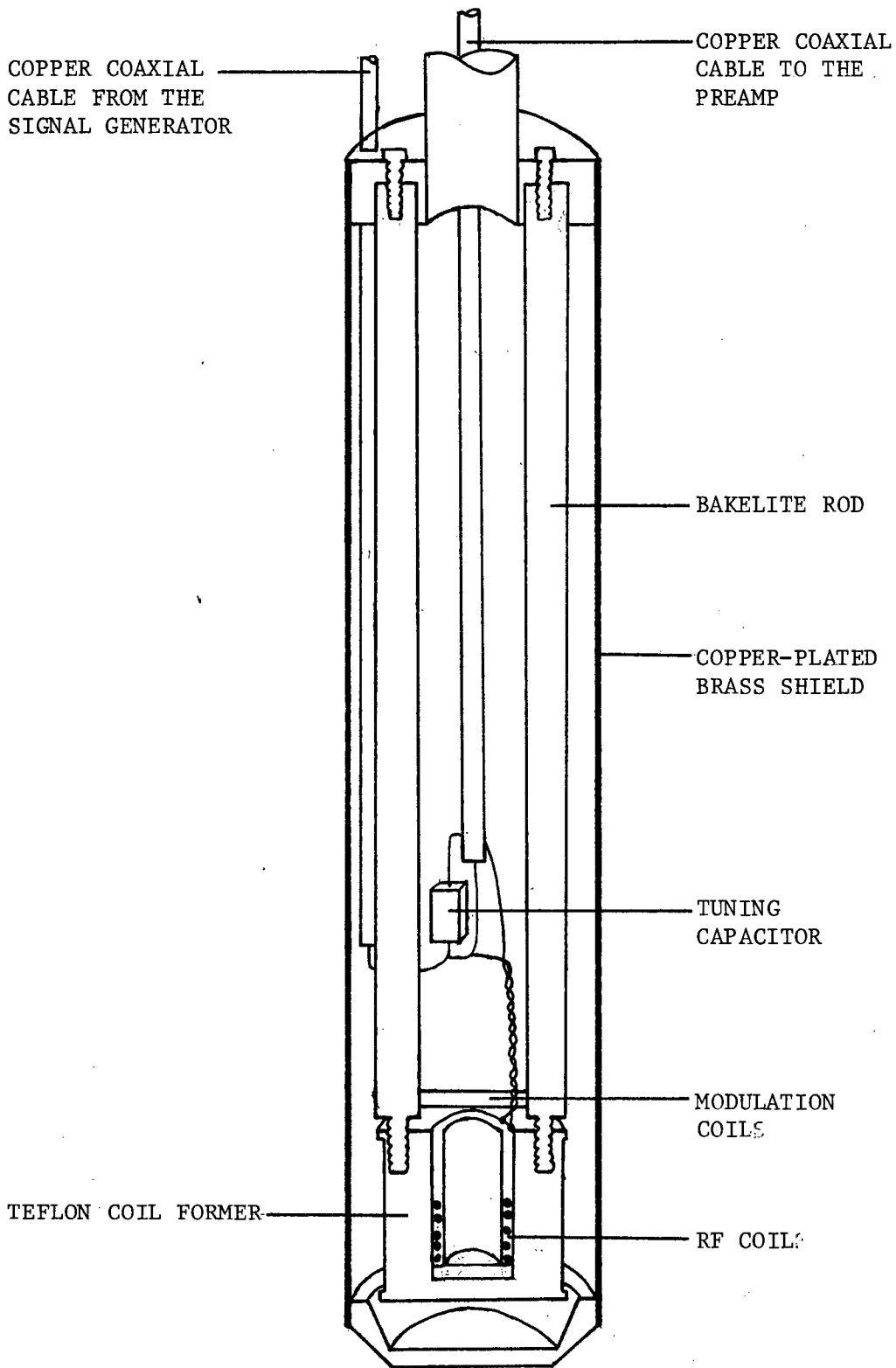


Figure 10) Schematic cut-away diagram of the bottom end of the cryostat.

The 400 pF tuning capacitance consisted of a 100 pF and a 300 pF rectangular silvered-mica capacitors (Sprague). The Q's were measured at room temperature to be about 1400 using an HP 4342A Q meter.

The RF coil consisted of 11 turns of bare 26 AWG copper wire wrapped on a thin, grooved Teflon cylinder. The coil was wrapped in Teflon tape and fit snugly inside the modulation coil form.

A 200 mg TTF-TCNQ powder sample was placed in a pyrex tube which had been drawn over a carbon mandril to reduce the wall thickness to .4 mm. The tubes were evacuated, filled with He gas and sealed. They fit snugly in the coil form when it was cooled to 77 K or below.

In order to minimize the noise figure of the preamp the impedance across its input must be real and it must be matched to the T1XM12 JFET's at the preamp input. The optimum source resistance is the value that makes the current noise equal to the voltage noise. At 4.2 K, for the particular devices used, it is 2.9 k Ω (Hardy and Gray, 1969). At 4.2 K, the tuned circuit has a Q of 850 giving it an equivalent parallel resistance of 41 k Ω . Since this greatly exceeds the optimum value, a matching network is required. The network used is shown in Fig. 11a. In the diagram:

R = equivalent parallel resistance of the tuned circuit

Z_i = impedance across the coil

Z_o = output impedance of the matching circuit

C₁ includes the capacitance of the coaxial cable from the matching circuit to the tuned circuit

C₃ includes the input capacitance of the preamp (\approx 7pF)

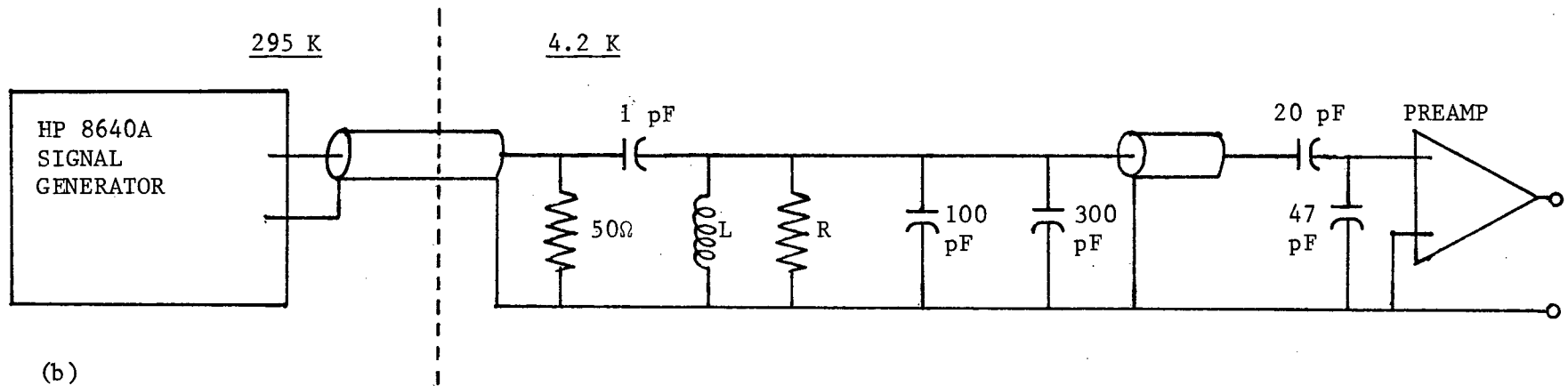
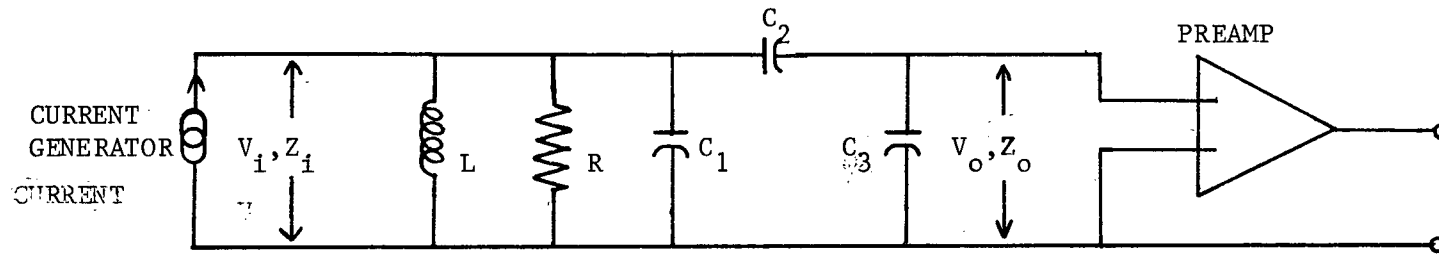


Figure 11) The tuned circuit and matching network.

It is easy to show that:

$$Z_i = \frac{Q}{\omega L + iQ(\omega L - \frac{1}{\omega C})} \quad \text{III-5}$$

$$\text{where } C = C_1 + \frac{C_2 C_3}{C_2 + C_3}$$

The resonance condition for V_i is $\omega^2 LC = 1$. Note that because the matching impedances are both capacitive, V_o is in phase with V_i and is also maximum when $\omega^2 LC = 1$. By straightforward but tedious calculation, one can obtain the following expression for Z_o :

$$Z_o = \frac{1 + iQ(\omega^2 L C_a - 1)}{i\omega C_b [1 + iQ(\omega^2 LC - 1)]} \quad \text{III-6}$$

$$\text{where } C_a = C_1 + C_2$$

$$C_b = C_2 + C_3$$

Note that although Z_i is real at resonance, Z_o is in general complex. However, it can be made approximately real by choosing C_2 and C_3 so that they satisfy:

$$R \gg \frac{C_2 + C_3}{\omega C_2^2}$$

C_2 and C_3 were chosen to be 20 pF and 54 pF respectively which made $Z_o = 2.9 \text{ k } \Omega$ at 4.2 K as required.

The results of the analysis above were confirmed at room temperature with an HP 4815 A RF Vector Impedance Meter since the value of the input capacitance of the preamp wasn't well known. The tuned circuit is shown in Fig. 11b. The 1 pF, 20 pF and 47 pF capacitors were Cornell-Dublier epoxy-dipped silvered mica. The 100 pF and 300 pF capacitors were rectangular Sprague silvered-

mica. The capacitance of the cable from the tuned circuit to the matching network was about 10 pF.

Some effort was expended in measuring the Q's of various capacitors at room temperature with an HP 4342 A Q-meter. Sprague rectangular silvered-mica capacitors had the highest Q's (about 1400). Cornell-Dublier rectangular silvered-mica capacitors had Q's almost as high. One might expect a capacitor with a Teflon dielectric to have a higher Q because the dissipation in Teflon is lower than in mica. However, we didn't have any Teflon capacitors. The Cornell-Dublier epoxy dipped silvered-mica capacitors had lower Q's than the rectangular ones - about 800 for the 20 pF and 47 pF capacitors and about 500 for the miniature 1 pF capacitor.

The 1 pF, 100 pF and 300 pF capacitors were non-magnetic. The 20 pF and 47 pF capacitors were magnetic but they were situated about 30 cm away from the RF coil.

4) Field Sweep and Modulation

It has already been mentioned that there are two basic approaches to making the bandwidth Δf of the detection system narrow. One can use a few slow sweeps with a long lock-in detector time constant or many fast sweeps with a short time constant. If the noise spectrum at the output of the lock-in is white and there is no saturation of the resonance signal, then the two techniques are equally efficient. In each case Δf^{-1} is proportional to the total observation time. However, fast scans actually have several advantages over slow scans. In practice noise isn't white: there is always excess noise at low frequencies. This type of noise amounts to a drift in the

baseline during a long scan but it is approximately constant during a short scan so it only results in a DC offset from one scan to the next. A single scan with a long time constant is more sensitive to strong but brief disturbances such as electrical equipment being turned on in another part of the room. If one uses the average of many scans, the effect of the disturbance will be slight because it appears on only one scan.

A further consideration is that in order to get maximum S:N one must saturate the resonance signal somewhat. The amount of saturation depends upon the amount of power applied and the length of time for which it is applied. By using many fast scans the spins are saturated evenly (if they all have the same saturation time) so that the magnitude of the signal decreases uniformly. On the other hand, in a slow scan some spins are saturated before the others so that the lineshape will be distorted. Finally, with fast scans one can watch the signal build up and stop the scans when saturation becomes too severe. If a single slow scan is used, the entire scan is wasted if saturation is too severe.

For the reasons cited above the fast scan technique appears to be considerably more attractive than the slow one. Originally we had intended to take the former method to its extreme limit by using sweep rates of 20-100 Hz and eliminating the lock-in detector and small modulation. By this method one obtains the absorption signal directly, rather than its derivative, so that there is an additional factor of $\sqrt{8}$ improvement in S:N.

A cryostat was built which was the same as the one described above apart from some modifications to the bottom end. The modulation coils weren't required so the diameter of the RF

coil could be larger. This increased its Q and more importantly the filling factor. Also the supporting rods for the Teflon coil form were copper rather than Bakelite. There were no H atoms near the RF coil. The sweep field was produced by pancake coils mounted on the pole faces of the magnet.

The cryostat just described was an unqualified disaster because of very severe microphonics that resulted from the interaction of eddy currents induced by the sweep field with the static magnetic field. The sweep coils produce eddy currents in any conductor between them so that the conductor will have an oscillating magnetic moment. Unless the shape of the conductor has a certain symmetry and the sweep field is exactly parallel to the static field \vec{H} , the magnetic moment will have a component perpendicular to \vec{H} . This induces a torque on the conductor causing it to move. Any motion of conductors near the RF coil causes a shift in the tuned circuit resonance frequency which results in amplitude modulation of the RF voltage across the coil. Since the induced magnetic moments have the same time dependence as the sweep field, coherent interference results.

This form of interference was particularly severe for the system described above. The Q was very high so that small shifts in the resonance frequency caused large amplitude modulation. In addition, the resonance signal was quite broad so large sweep fields, up to 100 G, were required. The pancake coils were quite large, in order to produce a homogeneous field, so that eddy currents were induced over the entire bottom end of the cryostat. Since the conductivity of the metal parts was high, particularly when the cryostat was cooled, the eddy currents were very large.

Although the coherent interference was worst at low temperatures, it was significant at room temperature as well. In fact if one simply held a brass rod in the magnet gap with the sweep coils and magnet on, there was noticeable vibration.

In order to reduce the coherent interference, the cryostat design was modified so that slow sweeps and small sinusoidal modulation with lock-in detection could be used. Metal parts near the RF coil were eliminated as much as possible. Small modulation coils mounted in the cryostat were used so that the modulation field extended over a much smaller region of the cryostat than the sweep field. The modulation field was only required to be about 1 G which is much less than the 100 G sweep field.

The cryostat was rotated to minimize the modulation pickup by aligning the axis of the modulation coils parallel to the static field. The pickup was further reduced by careful tuning of the signal generator frequency. When it is exactly equal to the tuned circuit resonance frequency, the amplitude modulation resulting from small shifts in the tuned circuit resonance frequency is zero to first order. The frequency was tuned by frequency modulating the signal generator at the lock-in detector reference frequency. For small modulation, the signal at the output of the lock-in detector was the derivative of the tuned circuit resonance curve and was a null at resonance.

Even with these precautions, the modulation pickup wasn't completely eliminated. However, it amounted to only a constant offset at the low RF and modulation amplitudes required for the TTF-TCNQ resonance signals at 4 K.

The field sweep circuit is shown in Fig. 9. The sweep coils, which were mounted on the pole faces of the magnet, were driven by a Kepco Bipolar Op-Amp 36-5M operated as a voltage controlled current source. The control voltage was the "sweep out" signal from the Fabritek 1062 Signal Averager. The "sweep out" voltage was proportional to the signal averager channel number. A .5 ohm Manganin wire resistor was used as the current sense resistor for the Kepco BOP since there was significant heating and hence change in resistance of the copper pancake coils. The manganin wire was heated too but it has a much lower temperature coefficient of resistivity than copper.

The Magnion FFC-4 Field Regulator controlled the magnetic field by comparing the signal from a rotating coil probe with a reference voltage. If the probe senses the sweep field, the magnet will regulate against it. One can prevent this by making the outer diameter of the sweep coils less than the diameter of the pole faces and positioning the probe so that it is in a region where the sweep field perpendicular to the probe is nearly zero. This is shown in Fig. 12.

The probe could be positioned so that it detected less than one thousandth of the sweep field at the sample. At that position, the static field sensed by the probe was about 500 G less than the field at the sample when a 13 kG field was applied.

The voltage across the manganin sense resistor, which is proportional to the current in the sweep coils, was used to trigger two marker pulses in the Sweep Marker Generator. These were added to the lock-in detector output before it went into the signal averager. The pulses allowed one to calibrate the sweep

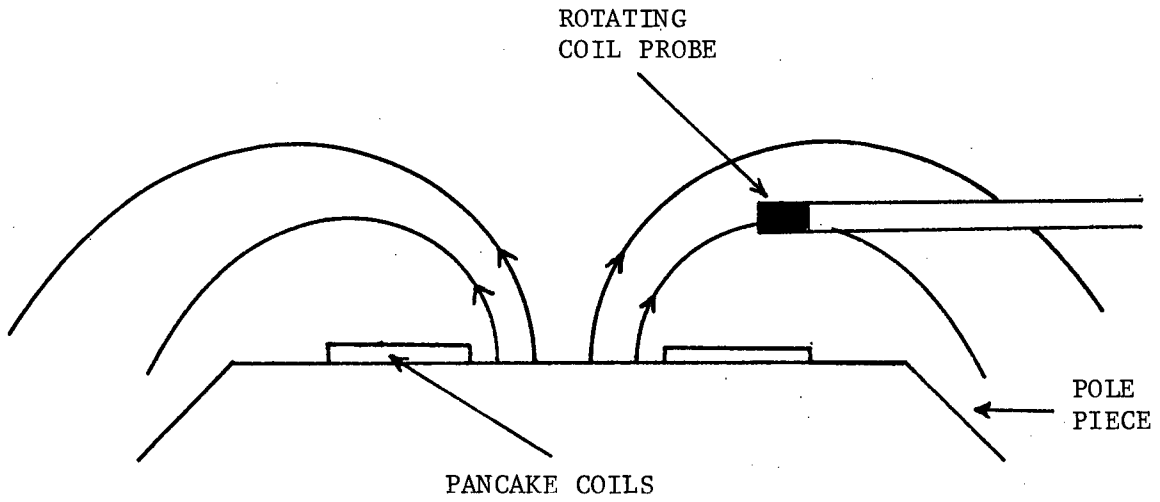


Figure 12) Position of the rotating coil probe so that the component of the field of the pancake coils perpendicular to the rotating coil probe is nulled.

and to check for drift in the sweep. No drift was ever observed so it must have been less than one channel width of the signal averager over several hours.

The sweep was calibrated as a function of the sense voltage and the linearity was checked using the DMR of D_2O at room temperature. The magnetic field was kept fixed and the frequency was changed. Since the tuned circuit had a fixed resonance frequency, a small amount of dispersion was mixed into the resonance signal when it was near the ends of the sweep.

The static magnetic field was calibrated during each run because the magnetic field differed by a few gauss each time it was turned on to 13 kG. The resonance signal of solid deuterium (33% para- D_2) at 4 K was used for this purpose.

5) Homogeneity

The linewidth of the DMR signal of TTF(d_0)-TCNQ(d_4) was narrow enough (2.8 G FWHM) that some care was required in positioning the sample in the magnet gap. It should be in the region of maximum homogeneity in order to minimize inhomogeneous broadening by the magnet. This was done at 4.2 K by varying the cryostat position until the best D_2 signal was obtained. Since the cryostat contracts by about 3 mm from room temperature to 4.2 K, the positioning had to be done at low temperature. First the best signal was obtained with no current in the sweep coils. A small sweep current was run through the modulation coils so that the resonance could be observed on an oscilloscope. Some fairly inhomogeneous shim coils were mounted on the pole faces of the magnet and the DC current through them was varied until the

best signal was obtained. The lineshape was not very sensitive to the shim coil current in the region of the maximum homogeneity. Then large positive and negative DC currents were run through the sweep coils and the resonance signal was observed in each case. The maximum currents that could be supplied by the Kepco op-amp were used, corresponding to fields of ± 80 G. The shim coil current was then varied. As one would expect, it wasn't possible to maximize the homogeneity at both ends of the sweep simultaneously so the best compromise was obtained. The lineshapes obtained with large DC currents in the sweep coils were much more sensitive to the shim coil current than the lineshape obtained with zero current in the sweep coils. Once the shim coil current was adjusted for the best homogeneity at the ends of the sweep, the increase in linewidth at the centre of the sweep was negligible. The signals at the ends of a ± 80 G sweep were $\sim 5\%$ broader than the signal at the centre.

The peak to peak linewidth of the derivative of the D_2 absorption signal was measured to be $1.69 \pm .05$ G. The measurement was made with $H_1 = .50$ mG and a modulation width of $.12$ G. At that RF level there was negligible saturation. The signal was slightly asymmetric, one peak being about 3% higher than the other. This seems to be an inhomogeneity effect.

W. N. Hardy (private communication) has given the linewidth as 1.7 G so the broadening due to the magnet inhomogeneity is insignificant. This conclusion is supported by the observation of the DMR signal of D_2O at room temperature. The linewidth was measured to be $.19$ G which is due entirely to the magnet inhomogeneity. Since the deuteron linewidth (FWHM) of TTF(d_0)-TCNQ(d_4) was 2.8 G the broadening due to the magnet inhomogeneity can be neglected.

Chapter IV

RESULTS

The low field half of the derivative of the deuteron absorption signal of TTF(d_0)-TCNQ(d_4) is shown in Fig. 13 and 14. Fig. 13 shows the main group of satellite peaks - the derivative of the shoulder and the singularity. Fig. 14 shows one of the small outer peaks - the derivative of the step. Fig. 15 was obtained by integrating the curve in Fig. 13 on the signal averager.

The spectra were obtained in a 13 kG magnetic field at a temperature of 1.3 K. At 1.3 K the deuteron spin-lattice relaxation time T_1 was of the order of 1600 s so very low RF levels were required to avoid saturation. Since T_1 is much greater than the time for a single scan (50 s), it is possible that although there is no noticeable saturation after a single scan, saturation may become substantial after several scans have accumulated in the signal averager. Fig. 13 was obtained from the accumulation of 42 scans of 50 s each at an RF level of $H_1 = .41$ mG. After the scans were completed, a single scan was made at higher RF and modulation levels. The signal was found to be badly distorted. However, while making the 42 scans the signal was recorded after 8, 16, and 32 scans. There was no noticeable increase in distortion between them so it seems that Fig. 13 is relatively undistorted. Other runs with lower S:N ratios have been made at RF levels down to $H_1 = .084$ mG. After these runs, a single scan at higher RF and modulation levels was undistorted so no significant distortion by saturation had occurred.

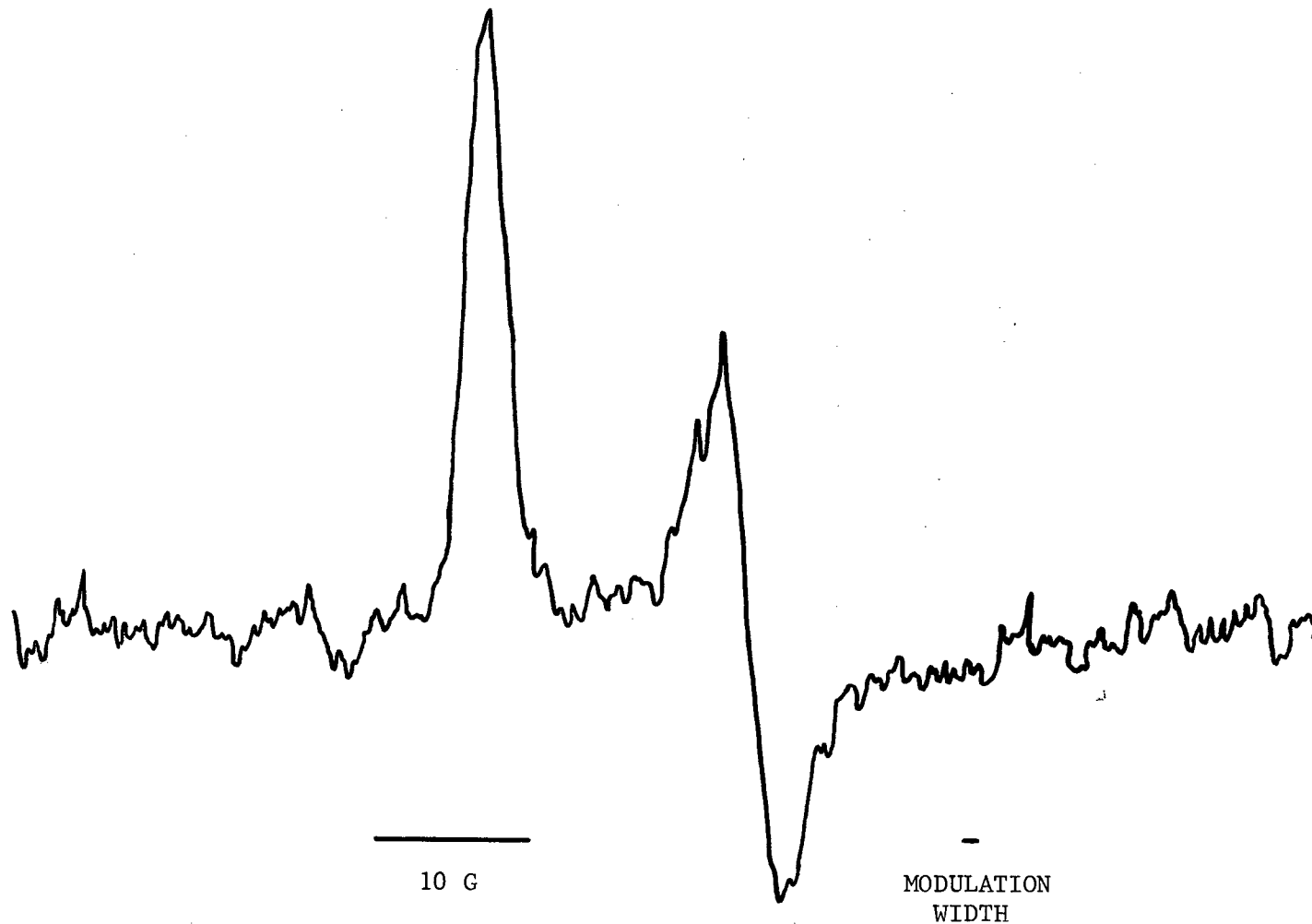


Figure 13) Low field main satellite peaks of TTF(d₀)-TCNQ(d₄) derivative DMR signal.
42 scans of 50 s each with H₁ = .41 mG.

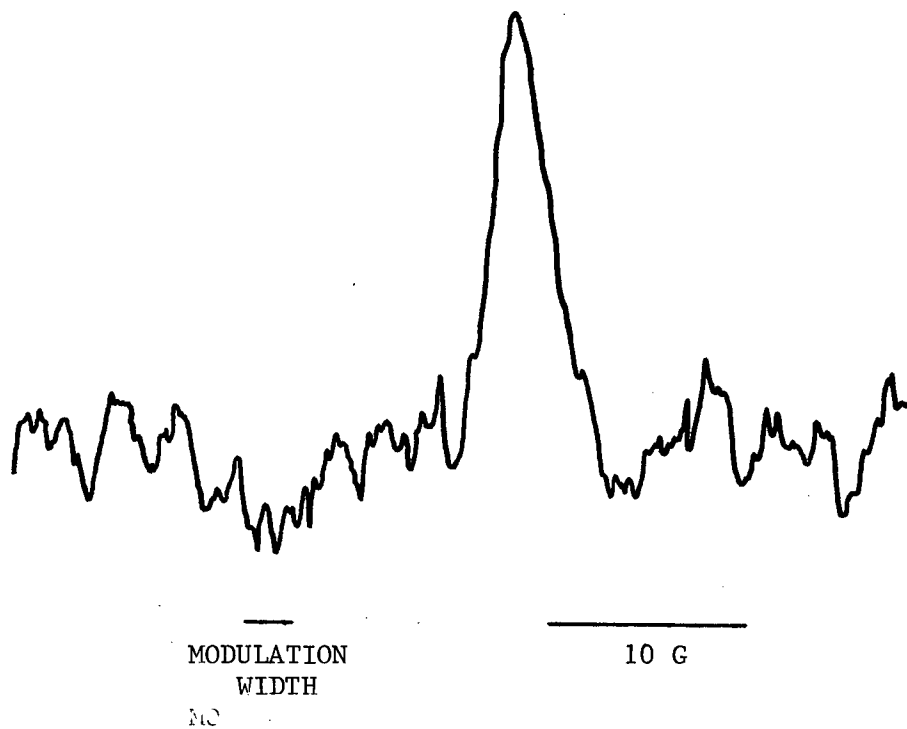


Figure 14). Low field outer peak of the TTF(d₀)-TCNQ(d₄) derivative DMR signal. 32 scans of 50 s each with H₁ = .39 mG.

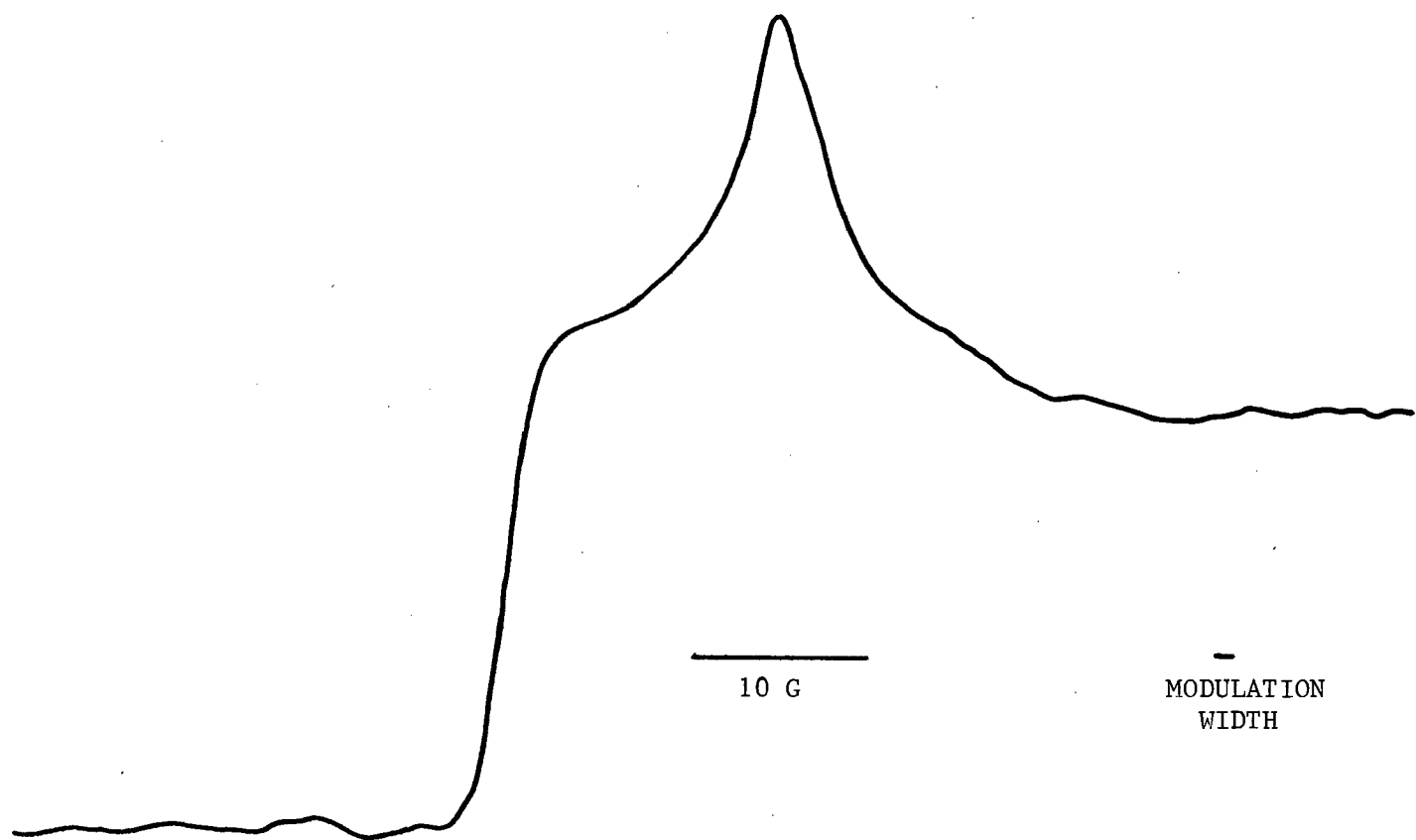


Figure 15) Integral of Fig. 13.

Comparison of these scans with Fig. 13 indicated that no significant distortion had occurred in Fig. 13.

The outer peak shown in Fig. 14 is the accumulation of 32 scans with $H_1 = .39$ mG. Because the outer peaks are much weaker than the main peaks it was necessary to increase the modulation amplitude over that used in Fig. 13 by a factor of two. This increased the linewidth by about 10%.

Comparison of Fig. 13-15 with Fig. 7 shows that the DMR spectrum of TTF-TCNQ(d_4) is quite similar to the computer generated spectra of Barnes and Bloom except that the homogeneous broadening of the TTF-TCNQ(d_4) signal is much less. There is no obvious manifestation of a CDW.

It was pointed out in Chapter I that at 54 K TTF-TCNQ undergoes a sinusoidal lattice distortion which is polarized primarily (or perhaps totally) along the b axis. The modulation period in the a direction depends upon the difference in phase of the distortion on adjacent TTF and TCNQ chains. Given that the modulation period in the b direction is $3.4 b$, these results are consistent with the model of a 1D conduction band with a charge transfer per molecule ρ such that:

$$\rho = \frac{b}{a} (2 k_F) = \frac{b}{a} \frac{2 \pi}{3.4b} = .59 \quad \text{IV-1}$$

One can get an estimate of the maximum possible effect of a CDW by comparing the QCC's of TCNQ(d_4) and TTF-TCNQ(d_4). The charge on the TCNQ^{-0.6} ion makes a contribution to the EFG not present in neutral TCNQ. Let us assume that below 38 K there is a pinned, incommensurate CDW along the TCNQ chains that consists

of a sinusoidal modulation of the charge density along those chains. Since the charge transferred from the TCNQ to the TTF goes into the 1D conduction band described above, the maximum possible amplitude of the CDW is equal to the difference in the average charge density in TCNQ^{-0.6} and neutral TCNQ.

Consequently we looked for the deuteron resonance signal of TCNQ(d₄). Fig. 16 shows the accumulation of 18 scans of 50 s each using an RF level of H₁ = .53 mG. The relaxation time wasn't measured because of the poor S:N ratio but judging from the saturation effects it appears to be of the order of an hour or more. There appears to be some distortion of the lineshape shown in Fig. 16 but it is only of the same magnitude as the noise.

One of the major reasons for the difficulties in observing the DMR of TTF-TCNQ(d₄) and TCNQ(d₄) is that T₁ is very long so low RF levels must be used. One can often shorten T₁ by introducing paramagnetic impurities which couple strongly to the lattice, having T₁'s of the order of 10⁻⁸ s. Their large local fields relax nearby nuclei which in turn relax their neighbours by spin diffusion.

Paramagnetic impurities can be introduced by irradiation with X- or γ-rays or by dissolving the sample with a paramagnetic salt and recrystallizing the solute. The main stumbling blocks are that in the former case recombination may occur and in the latter case the two components may recrystallize separately. If large concentrations of impurities are introduced, the DMR signal will be broadened.

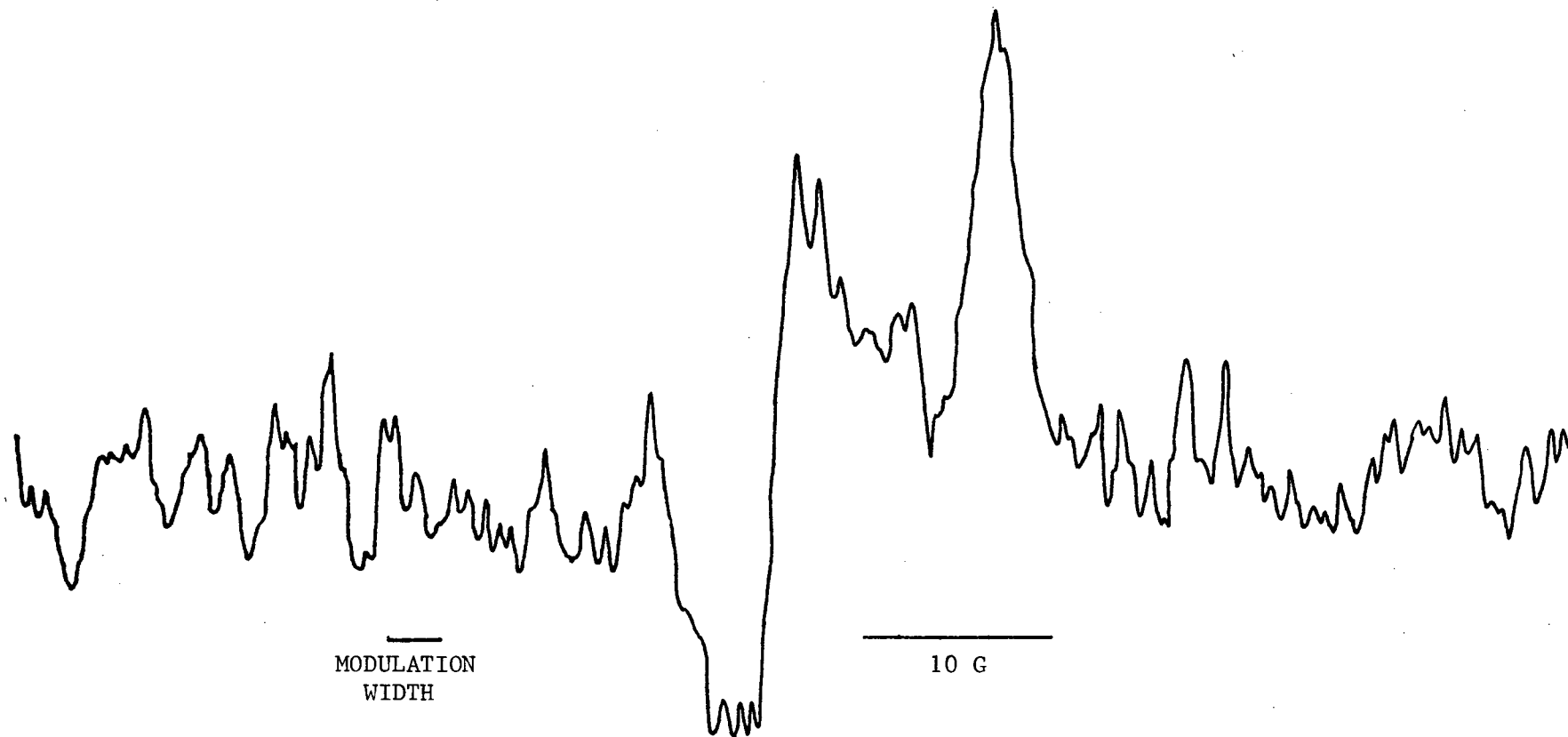


Figure 16) High field main satellite peaks of TCNQ(d₄) derivative DMR signal. 18 scans of 50 s each with H₁ = .53 mG.

Several unsuccessful attempts were made to observe the TCNQ(d₄) signal using a different cryostat from the one described above. The sample was irradiated for up to 9 hours with 120 keV X-rays with no apparent effect. In order to slow down possible recombination, the sample was irradiated while cooled by liquid nitrogen and immediately afterward placed in a cryostat cooled to 77 K. The sample was only exposed to temperatures above 77 K for a few seconds when it was transferred from the liquid nitrogen bath to the cryostat. This was also ineffectual.

More recently, after the TCNQ(d₄) signal had been observed, an attempt was made to dope the sample with Mn⁺² to improve the S:N. Mn [TCNQ(d₄)]₂ was made, dissolved with TCNQ(d₄) and the solute recrystallized. Enough Mn was used to give concentrations of .01% Mn (by weight) and .05% Mn on two different occasions. It isn't known how many of the impurities actually went into the new crystals though. The colour of the crystals (orange-brown) was unchanged. There was no distinct improvement in the signal.

We have obtained values of the QCC and η from the peak positions of the DMR signals as described in Chapter II. These are shown in Table I.

Table I

Quadrupole Coupling Constants
and Asymmetry Parameters

<u>Sample</u>	<u>e^2qQ/h (kHz)</u>		<u>T(K)</u>
TTF (d ₀) -TCNQ (d ₄)	180.0 ± .7	.080 ± .002	1.3
TCNQ (d ₄)	167.0 ± .9	.061 ± .005	4.2

The difference in the QCC's for the neutral and charged TCNQ is 13 kHz. Therefore according to our previous discussion, the maximum range of QCC's that could be produced by a CDW is 26 kHz. Experimentally, the resolution is limited by the broadening. As a first estimate this is given by the FWHM of the main peak of Fig. 13 which is 1.8 ± 0.2 kHz. This value has been corrected for the width of the modulation (Andrew, 1953). Since the broadening is relatively small, the main peak is well separated from the other features so its width should not be affected by η very much.

The effect of a plane, sinusoidal, incommensurate CDW on a quadrupolar lineshape was shown in Fig. 8. If one assumes a two peaked distribution of this form in TTF-TCNQ and gaussian broadening, then it should be possible to resolve the peaks if their splitting is greater than about twice the standard deviation, σ , of the broadening function. The sum of two gaussian peaks, each with a standard deviation σ , can be resolved under these conditions. If their separation is equal to 2σ , then a single peaked function with a FWHM $\approx 4\sigma$ results. Therefore in TTF-TCNQ, with these assumptions, it should be possible to resolve a distribution equal to one half of the FWHM. The limit of resolution for a distribution of QCC's would then be $(1/2)(8/3)(1.8) = 2.4$ kHz from the width of the main peaks.

Actually a CDW would not be a plane wave in TTF-TCNQ. However, only the EFG at the deuteron sites is important. Neutron scattering indicates that the CDW should be sinusoidal along the chains. If the deuterons are equivalent, then at their sites along a chain the EFG should be the same as if the CDW were a plane wave. It is shown in Chapter V that the dipolar broadening is not expected to be gaussian. The estimate of the limit of resolution given above may not be valid then. In any event the distribution of QCC's could be at most twice as much if it were responsible for all of the broadening.

Chapter V

SOURCES OF BROADENING

Although there is no obvious distribution of QCC's in the experimental DMR spectrum of TTF-TCNQ(d₄), it remains to consider whether the broadening can be accounted for by the dipole-dipole interactions between the spins or whether it may be due to an unresolved splitting. If one assumes a rigid lattice model containing only one type of spin, then the second moment for the dipolar broadening is (Abragam, 1961):

$$\langle \Delta H^2 \rangle_{II} = \gamma_I^2 \hbar^2 I(I+1) \sum_{k \neq j} \frac{(1 - 3\cos^2 \theta_{jk})^2}{r_{jk}^6} \quad V-1$$

where \vec{r}_{jk} is the position vector between spins j and k and θ_{jk} is the angle between \vec{r}_{jk} and \vec{H} . All spins are assumed to be equivalent.

For a powder with randomly oriented crystallites this becomes:

$$\langle \Delta H^2 \rangle_{II} = (3/5) \gamma_I^2 \hbar^2 I(I+1) \sum_{k \neq j} r_{jk}^{-6} \quad V-2$$

Before applying this technique to the deuteron linewidth, its validity was checked using the proton resonance of TTF(d₄)-TCNQ(d₀). $\langle \Delta H^2 \rangle_{II}$ was calculated considering only the dipole-dipole interactions between protons. The contribution to $\langle \Delta H^2 \rangle_{HH}$ from protons on the same molecule is 3.08 G²; 97% is from the

nearest proton alone. The contribution from the protons on the two nearest neighbour molecules on the same chain is $.64 \text{ G}^2$. All other dipole-dipole interactions (including H-D and H-N) are insignificant so the calculated square root of the proton second moment is 1.93 G .

The experimental proton absorption signal from TTF(d₄)-TCNQ(d₀) is shown in Fig. 17. The lineshape is characteristic of a system in which the shortest H-H distance is much less than all other H-H distances. The dipole-dipole interaction of a proton with its nearest neighbour then makes the dominant contribution to the second moment. This was seen to be the case in the calculation above. The square root of the second moment was measured to be 1.60 G using a 36 point numerical integration of the lineshape over a 12 G range. A correction was made for the residual proton signal with the sample removed. The agreement between the measured and calculated values is moderately good. The discrepancy presumably arises because the contribution to the experimental value from the wings was buried in noise. The peak to peak separation of the derivative signal was $3.77 \pm .07 \text{ G}$ which compares fairly well with the value of 4.0 G given by Rybaczewski (1974).

Using equation V-2 one can estimate the broadening if the protons are replaced by deuterons. Equation V-2 implies that if the lineshapes are gaussian, then the ratio of the deuteron dipolar linewidth to that of the protons is:

$$\frac{\gamma_D}{\gamma_P} \left(\frac{I_D(I_D + 1)}{I_P(I_P + 1)} \right)^{1/2} = .25 \quad \text{V-3}$$

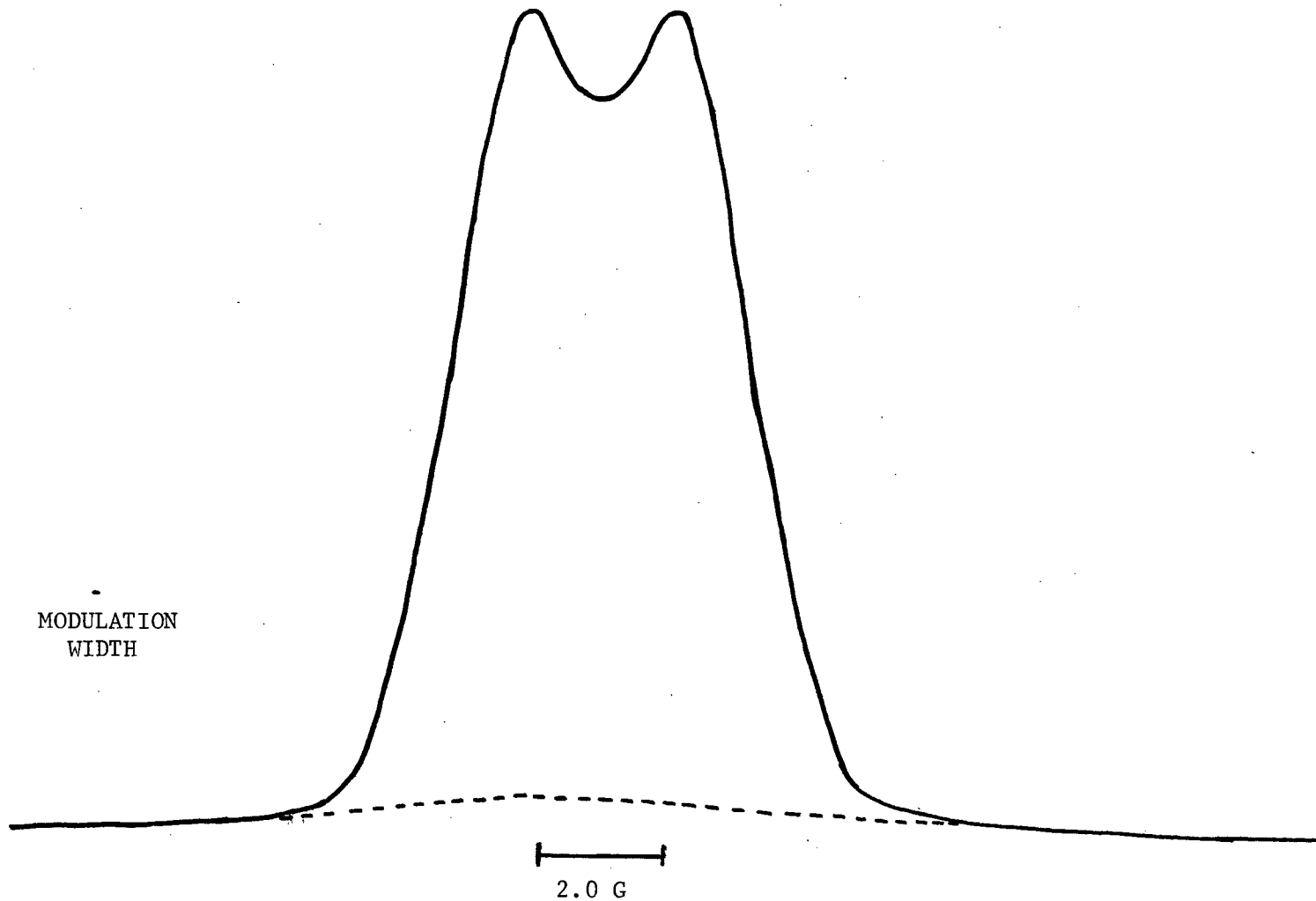


Figure 17) Proton absorption signal of $\text{TTF}(\text{d}_4)\text{-TCNQ}(\text{d}_0)$. $H_1 = .21 \text{ mG}$. The residual proton signal with no sample is shown by the dashed line.

The experimental deuteron linewidth can be obtained from the width of the main peak in Fig. 13 which is $2.8 \pm .3$ G FWHM. Using the experimental value of the proton FWHM which is 4.60 G, equation V-3 gives an expected value of 1.15 G for the deuteron FWHM; there is a factor of 2.4 discrepancy. The proton signal is not gaussian so the deuteron lineshape shouldn't be either. However, considering the S:N ratio of the deuteron signal this approximation is reasonable. Despite the inadequacies of the calculation above, the discrepancy seems rather large.

Apart from CDW effects, there are two other possible sources of additional broadening that will be discussed below. First, the ratio of the proton magnetic moment to that of the deuteron is 6.51. Consequently other species of spins will have a much greater effect on the deuteron dipolar broadening than on that of the protons. Secondly, some of the deuteron sites may be inequivalent.

In the following discussion molecules will be labelled by the positions of their centroids using the crystal axes as coordinate axes. This coordinate system is shown in Fig. 4. The atoms on each molecule are labelled as in Fig. 3. For example H(8) on TCNQ at $(a/2, 0, 0)$ means the H atom at position 8 (see Fig. 3) of the TCNQ molecule whose centroid is located at $(a/2, 0, 0)$ (see Fig. 4). All interatomic distances are obtained from the X-ray diffraction data of Kistenmacher, Phillips and Cowan (1974).

Consider a crystal of TTF(d_0)-TCNQ(d_4). Using the same dipole-dipole interactions as in the calculation of $\langle \Delta H^2 \rangle_{HH}$ above, one finds that $\langle \Delta H^2 \rangle_{DD} = .233 \text{ G}^2$. The protons on the

TTF molecules will make an additional contribution. The effect of protons on the deuteron second moment is given by (Abragam, 1961).

$$\langle \Delta H^2 \rangle_{PD} = \frac{4}{15} \gamma_P^2 \hbar^2 I_P (I_P + 1) \sum_k r_{jk}^{-6} \quad \text{V-4}$$

Consider D(8) on TCNQ at $(a/2, 0, 0)$. The nearest proton is H(2) on TTF at $(0, b, 0)$ (4.39 Å separation) and the second nearest is H(2) on TTF at $(0, 0, 0)$ (4.58 Å separation). The protons H(1') on the same molecules are a little farther away. All others are far enough away that their contribution isn't very significant. Therefore a reasonable estimate of the proton contribution would be to take twice the effect of the two nearest protons. If one does this the result is $\langle \Delta H^2 \rangle_{PD} = .086 \text{ G}^2$. This only increases $\langle \Delta H^2 \rangle^{1/2}$ by 17%. It cannot account for more than a small part of the extra broadening of the deuteron lineshape.

The N^{14} nuclei also make a contribution to the deuteron second moment. The effect of the nearest N^{14} nucleus (separation is 2.91 Å) is $\langle \Delta H^2 \rangle_{ND} = .0037 \text{ G}^2$. Since all other N^{14} nuclei are considerably farther away, this contribution is insignificant.

It is now necessary to consider whether all of the deuteron sites are equivalent. Fig. 6c shows that for a powder sample the spectrum depends only upon e_q and η : it is averaged over all orientations of the principal axes with respect to \vec{H} . Thus in a powder two sites are inequivalent only if they have different values of e_q or η .

The maximum component of the EFG tensor in the principal axis system, eq , can be written as the sum of nuclear and electronic contributions.

$$eq = e \sum_k Z_k (3 \cos^2 \theta_k - 1) r_k^{-3} - e \sum_j \langle \psi | (3 \cos^2 \theta_j - 1) r_j^{-3} | \psi \rangle$$

$$= eq_n - eq_e$$

V-5

where k denotes nuclei, j denotes electrons, Z_k is the charge of the k^{th} nucleus, \vec{r}_k is its position, θ_k is the angle between \vec{r}_k and the principal z axis, and ψ is the electronic wave function.

In TTF-TCNQ all H atoms are bonded to C atoms so the dominant nuclear contribution to eq at the H atom is from the C atom. Typically for C-D bonds the carbon nucleus gives 90% of the nuclear contribution to eq (Rinné and Depireux, 1972). The contribution of the $1s$ orbital of the deuteron to eq_e is zero because that orbital is spherically symmetric. The deuteron $2p$ orbitals are too high in energy to be occupied to any appreciable extent so the deuteron orbitals make no contribution to eq_e . The dominant contribution to eq_e is from the C orbitals. Typically over 70% of eq_e arises from the C-D bonding orbital alone (Rinné and Depireux, 1972).

In many cases eq_n can be calculated quite accurately, it is always positive. $|eq|$ is always found to be smaller than eq_n so eq_e must also be positive. In all cases where the sign of the deuteron QCC has been determined experimentally it has been positive. Since the quadrupole moment Q of the deuteron is also positive, eq_n must always be greater than eq_e . Typically the electrons shield 80% of the EFG produced by the C nucleus in a

C-D bond (Bersohn, 1960). Since eq arises from the near cancellation of two terms it is very sensitive to small changes in the electronic charge density.

One might have expected the QCC of the $\text{TCNQ}^{-.6}$ ion to be smaller than that of neutral TCNQ. Since $\text{TCNQ}^{-.6}$ has additional electronic charge as compared with neutral TCNQ, it seems reasonable to expect that the electronic contribution to eq would be larger in the former. This would make eq smaller according to equation V-5 whereas Table I shows that it is larger. However, there seems to be no relation between the QCC and the formal charge on an ion (Olympia, Wei, and Fung, 1969). For example ND_4^+ has a lower deuteron QCC than ND_3 .

In an isolated molecule of TCNQ all of the deuterons are equivalent; i.e., they have the same eq and η . Fig. 4 shows that for a given TCNQ molecule in a $\text{TTF}(d_0)\text{-TCNQ}(d_4)$ crystal, D(8) and D(8') are equivalent and D(9) and D(9') are equivalent but D(8) and D(9) are inequivalent. For adjacent molecules along the C axis (one of which is denoted by an asterisk), H(8) and H(8')* are equivalent as are H(9) and H(9')*. Therefore in the crystal as a whole there are two inequivalent sites. The inequivalence arises because the a and c axes are not orthogonal. Since one normally expects eq to be determined by the C nucleus and C orbitals, the inequivalence should be small.

The inequivalence of the deuterons on the TCNQ molecules arises primarily from interactions with the two adjacent rows along the a axis. One can estimate the amount of the inequivalence caused by molecules in these rows by calculating the EFG's using a point charge model. Using a Mulliken population analysis (Mulliken, 1955), one can obtain a model in

which the electrons are distributed among the atomic orbitals of the molecules. From this distribution, one can obtain the "gross atomic charge", c , for each atom. The EFG at a point in a neighbouring molecule can then be estimated by treating the gross atomic charges as point charges located at the centres of their respective atoms.

The gross atomic charges for TTF^0 , TTF^{-1} , TCNQ^0 , TCNQ^{-1} and TCNQ^{-2} have been determined from self consistent field molecular orbital calculations (Ratner, 1974 and Johansen, 1975). The results are summarized in Table II.

Table II

Gross Atomic Charges e^-

A) TCNQ

Atom	TCNQ ⁰	TCNQ ⁻¹	TCNQ ⁻²
C(9)	-.04	-.06	-.08
C(7)	.10	.07	.03
C(6)	.07	-.06	-.17
C(5)	-.16	-.15	-.14
N(2)	-.03	-.15	-.26
H(9)	.14	.10	.05

B) TTF

Atom	TTF ⁰	TTF ⁺
S(1)	.018	.185
C(1)	-.024	-.006
C(3)	-.005	.116

The TCNQ data shows that the gross atomic charges scale with the charge on the molecules. This will be assumed to be also true for TTF. It should be pointed out that the absolute values of the gross charges generally depend strongly on the set of basis functions used. The relative values for the same molecule with different charges are usually fairly consistent though. The only experimental confirmation of these calculations is the N^{14} NMR data. Murgich and Pissanetzky (1973) found that the increase in charge on K-TCNQ as compared with neutral TCNQ is .13 e. This agrees quite well with Johansen's calculated value of .12 e.

If one scales the values of c given in Table II to a molecular charge of .6, one finds that in $TCNQ^{-.6}$ the negative charge is predominantly on the CN groups while in $TTF^{.6}$ the positive charge is predominantly on the sulfur and the central carbons. Only these charges were used in the EFG calculation below. The outer C atoms of TTF are almost neutral.

Consider the inequivalent deuterons D(8') and D(9') on TCNQ at $(a/2, b/2, c/2)$. The point charges primarily responsible for the inequivalence are located on the TCNQ molecule at $(a/2, 0, 0)$ and the TTF molecule at $(0, b, 0)$. Charges on other molecules will make fairly small contributions because the EFG has an r^{-3} dependence. Considering the accuracy of the absolute values of c , it is pointless to include these other charges.

Since the C nucleus and C-D bonding orbital provide the dominant contributions to the deuteron EFG, the z axis of the principal axis system can be approximated very well by the C-D bond axis. Furthermore since the EFG produced by the point

charges on neighbouring molecules is a small perturbation, one only needs to consider its V_{ZZ} component. Other components have only a second order effect.

The contributions to eq at each of D(8') and D(9') on TCNQ at $(a/2, b/2, c/2)$ from the point charges located at N(1), N(2), C(4), and C(5) on $(a/2, 0, 0)$ and at S(1), S(2), and C(3) on TTF at $(0, b, 0)$ have been calculated. The results are:

$$q [D(8')] = -2.1 \times 10^{21} \text{ cm}^{-3}$$

$$q [D(9')] = .8 \times 10^{21} \text{ cm}^{-3}$$

This difference would produce a distribution in e^2qQ/h equal to .29 kHz, and hence a broadening of $(3/8)(2\pi/\gamma)(.29) = .17$ G in the main peak which is much less than the observed width of 2.8 G. One concludes that the extra broadening cannot be caused by the existence of two inequivalent sites.

CHAPTER VI

CONCLUSIONS

The calculations of Chapter V indicate that the width of the DMR signal of TTF(d_0)-TCNQ(d_4) cannot be accounted for by either the dipolar broadening or the inequivalence of the deuteron sites. One is tempted to ascribe the broadening to a distribution of QCC's caused by a CDW. However, there is a fundamental difficulty with doing this. Fig. 7b shows that the splitting between the two outer peaks of the DMR spectrum is $f_Q = (3/2)e^2qQ/h$ whereas between the two main peaks it is $(1/2)f_Q(1+\eta) \approx (1/2)f_Q$ for TTF-TCNQ since $\eta \ll 1$. Therefore a distribution of EFG's would cause twice as much broadening in the outer peaks as in the main ones. The measured FWHM's are $2.8 \pm .3$ G for the main peaks and ≈ 3.1 G for the outer peaks after correcting for the width of the modulation (Andrew, 1953). The difference is only of the order of the experimental error. It is by no means large enough to allow one to attribute the width of the main peaks to a distribution of QCC's.

The difference in the widths, if it is significant, can probably be accounted for by the small inequivalence of the deuteron sites discussed in Chapter V. The result of the calculation there implied a distribution of QCC's of the order of .29 kHz wide. This would imply a broadening of the main peaks by $(3/8)(2\pi/\gamma)(.29) = .17$ G and of the outer peaks by twice as much— .34 G. This mechanism would cause the outer peaks to be .17 G wider than the main ones. It seems that the difference in the widths of the peaks can be accounted for without invoking the existence of a CDW.

Although there is no evidence of the existence of a CDW, one can put an upper limit on the amplitude of a CDW if one did exist using the FWHM of the outer peak which is 2.0 kHz. In accordance with the argument at the end of Chapter IV, if one assumes that a distribution of QCC's equal to one half of the FWHM could be resolved, then the limit of resolution for a distribution of QCC's is $(1/2)(4/3)(2.0) = 1.3$ kHz. From a comparison of the QCC's of $\text{TCNQ}(d_4)$ and $\text{TTF}(d_0) - \text{TCNQ}(d_4)$, the discussion of Chapter IV suggested that the maximum range of QCC's a CDW could produce is 26 kHz. Therefore an estimate of the maximum possible amplitude of a CDW on the TCNQ chains is $\sim 5\%$.

BIBLIOGRAPHY

- Abragam, A, THE PRINCIPLES OF NUCLEAR MAGNETISM, Oxford University Press, London (1961)
- Andre, JJ, Bieber, A, and Gautier, F, Ann. Phys., 1, 145 (1976)
- Andrew, ER, Phys. Rev., 91, 425 (1953)
- Andrew, ER, NUCLEAR MAGNETIC RESONANCE, Cambridge University Press, Cambridge (1955)
- Barnes, RG, Adv. in NQR, 1, 335 (1972)
- Barnes, RG, and Bloom, JW, J. Chem. Phys., 57, 3082 (1972)
- Berlinsky, AJ, Contemp. Phys., 17, 331 (1976)
- Berlinsky, AJ, Carolan, JF, and Weiler, L, Sol. St. Comm., 15, 795 (1974)
- Bersohn, R, J. Chem. Phys., 32, 85, (1960)
- Chaikin, PM, Kwak, JF, Jones, TE, Garito, AF, Heeger, AJ, Phys. Rev. Lett., 31, 601 (1973)
- Cohen, MH, and Reif, F, SOLID STATE PHYSICS, 5, ed. Seitz and Turnbull, (1957)
- Comès, R, Shirane, G, Shapiro, SM, Garito, AF, and Heeger, AJ, Phys. Rev. B, 14, 2376 (1976)
- Craven, RA, Salomon, MB, De Pasquali, G, Herman, RM, Stucky, G, Schultz, A, Phys. Rev. Lett., 32, 769 (1974)
- Denoyer, F, Comès, R, Garito, AF, Heeger, AJ, Phys. Rev. Lett., 35, 445 (1975)
- Djurek, D, Franulović, K, Prester, M, Tomić, S, Giral, L, Fabre, JM, Phys. Rev. Lett., 38, 715 (1977)
- Follstaedt, D and Slichter, CP, Phys. Rev. B, 13, 1017 (1975)
- Hardy, WN and Gray, KW, A Study of Noise in Field-Effect Transistors at Low Temperatures, North American Rockwell Technical Report, unpublished, (1969)
- Kagoshima, S, Anzai, H, Kajimura, K, Ishiguro, T, J. Phys. Soc. Jap., 39, 1143 (1975)

- Kistenmacher, TJ, Phillips, TE, and Cowan, DO, Acta. Cryst.,
B 30, 763 (1974)
- Kohn, W, Phys. Rev. Lett., 2, 393 (1959)
- Johansen, H, Int. J. Quant. Chem., IX, 459 (1975)
- Landau, LD, and Lifshitz, EM, STATISTICAL PHYSICS, §152,
Addison-Wesley, London, Ontario (1969)
- Mulliken, RS, J. Chem. Phys., 23, 1833 (1955)
- Murgich, J and Pissanetzky, S, Chem. Phys. Lett., 18, 420 (1973)
- Olympia, PL Jr., Wei, YI, Fung, BM, J. Chem. Phys., 51, 1610
(1969)
- Peierls, RE, QUANTUM THEORY OF SOLIDS, Oxford University
Press, London, (1955)
- Pincus, P, LOW DIMENSIONAL COOPERATIVE PHENOMENA, ed. HJ Keller,
Plenum Press, New York (1975)
- Ratner, MA, Sabin, JR, Ball, EE, Chem. Phys. Lett., 28, 393
(1974)
- Rinné, M and Depireux, J, Adv. in NQR, 1, 357 (1972)
- Rybczewski, EF, PhD Thesis, U. of Pennsylvania, unpublished
(1974)
- Scott, JC, Garito, AF, and Heeger, AJ, Phys. Rev. B 10, 3131
(1974)
- Slichter, CP, PRINCIPLES OF MAGNETIC RESONANCE, Harper and
Row, New York (1963)
- Tiedje, T, Master's Thesis, U. of British Columbia, unpublished
(1975)